1994-09

An initial assessment of free surface effects on submerged bodies

Crook, Thomas P.

Monterey, California. Naval Postgraduate School

NAVAL POSTGRADUATE SCHOOL
Monterey, California

THESIS

AN INITIAL ASSESSMENT OF
FREE SURFACE EFFECTS ON
SUBMERGED BODIES

by

Thomas P. Crook

September, 1994

Thesis Advisor: Fotis A. Papoulias

REPORT DOCUMENTATION PAGE

Form Approved OMB No. 0704

1. AGENCY USE ONLY	2. REPORT DATE	3. REPORT TYPE AND DATES COVERED
	September 1994.	Master's Thesis

4. TITLE AND SUBTITLE AN INITIAL ASSESSMENT OF FREE SURFACE EFFECTS ON SUBMERGED BODIES

5. FUNDING NUMBERS

6. AUTHOR(S) CROOK, Thomas P.

7. PERFORMING ORGANIZATION NAME(S) AND ADDRESS(ES)
Naval Postgraduate School
Monterey CA 93943-5000

8. PERFORMING ORGANIZATION REPORT NUMBER

9. SPONSORING/MONITORING AGENCY NAME(S) AND ADDRESS(ES)

10. SPONSORING/MONITORING AGENCY REPORT NUMBER

11. SUPPLEMENTARY NOTES The views expressed in this thesis are those of the author and do not reflect the official policy or position of the Department of Defense or the U.S. Government.

12a. DISTRIBUTION/AVAILABILITY STATEMENT
Approved for public release; distribution is unlimited.

12b. DISTRIBUTION CODE
*A

13. ABSTRACT
This thesis presents a study of free surface effects on submerged bodies. The motivation for this study lies in the significance of free surface suction effects during submarine operations at periscope depth. Such operations become increasingly important as new roles for the Navy in littoral waters are emerging. Particular emphasis is placed on computation of steady state forces on the body as a function of speed, depth, and wave frequency and direction. These forces constitute an important and very frequently limiting factor in establishing the periscope depth submerged operating envelope. Solution of the problem is accomplished by singularity distribution on the actual surface of the body and discretization in the form of plane quadrilateral elements. Parametric studies are conducted in order to assess the effects of body shape and size. The results of this thesis can be directly utilized in the simulation based design process as well as during training.

14. SUBJECT TERMS Submarine, periscope depth, wave making, incident waves, potential flow

15. NUMBER OF PAGES *109

16. PRICE CODE

17. SECURITY CLASSIFICATION OF REPORT	18. SECURITY CLASSIFICATION OF THIS PAGE	19. SECURITY CLASSIFICATION OF ABSTRACT	20. LIMITATION OF ABSTRACT
Unclassified	Unclassified	Unclassified	UL

NSN 7540-01-280-5500

Standard Form 298 (Rev. 2-89)
Prescribed by ANSI Std. 239-18

Approved for public release; distribution is unlimited.

AN INITIAL ASSESSMENT OF FREE SURFACE EFFECTS ON SUBMERGED BODIES

by

Thomas P. Crook
Lieutenant Commander, United States Navy
B.S., United States Naval Academy, 1982

Submitted in partial fulfillment
of the requirements for the degree of

MASTER OF SCIENCE IN MECHANICAL ENGINEERING

from the

NAVAL POSTGRADUATE SCHOOL
September 1994

Author: [redacted]

Thomas P. Crook

Approved by: [redacted]

Fotis A. Papoulias, Thesis Advisor

[redacted]

Matthew D. Kelleher, Chairman
Department of Mechanical Engineering

ABSTRACT

The motivation for this study lies in the significance of free surface suction effects during submarine operations at periscope depth. Such operations become increasingly important as new roles for the Navy in littoral waters are emerging. Particular emphasis is placed on computation of steady state forces on the body as a function of speed, depth, and wave frequency and direction. These forces constitute an important and very frequently limiting factor in establishing the periscope depth submerged operating envelope. Solution of the problem is accomplished by singularity distribution on the actual surface of the body and discretization in the form of plane quadrilateral elements. Parametric studies are conducted in order to assess the effects of body shape and size. The results of this thesis can be directly utilized in the simulation based design process as well as during training.

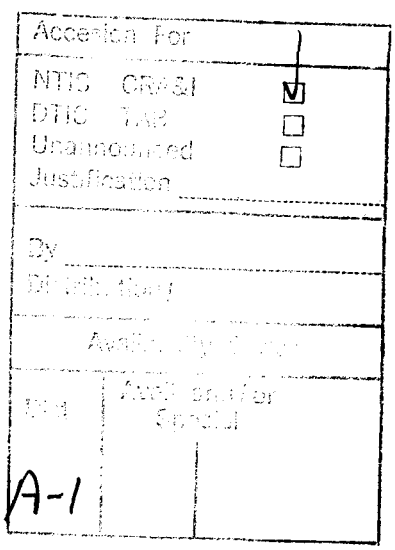

TABLE OF CONTENTS

ACKNOWLEDGMENT

First and foremost, I acknowledge the continuing faithfulness of my Lord and Saviour, Jesus Christ. He is always there and His mercies are new every morning.

Secondly, my deepest thanks for the loving support of my dearest wife, Greta, and my three precious children, Jonathan, Joseph, and Deenalin. Theirs is a constant expression of lovingkindness.

Finally, my highest appreciation to Professor Fotis A. Papoulias, for his expert guidance and excellent instruction during the course of this thesis.

I. INTRODUCTION

Submarine missions are rapidly evolving into frequent deployments to littoral areas, which require operating in shallow water. Shallow water is usually defined as a charted depth of less than 600 feet, but can be as shallow as 180 feet or less in certain situations. Shallow water operations sharply contrast with the traditional, blue water missions of the Cold War. Instead of concentrating on anti-submarine warfare (ASW) against modern Soviet platforms, submarines will execute ASW against older, diesel submarines operating in littoral areas. Also, surveillance (both visual and electronic) operations, mine laying evolutions, and joint special forces' expeditions will become routine occurrences as the submarine force responds to dynamic regional conflicts.

Given the abundant time submarines will spend operating in shallow water, the importance of periscope depth operations greatly expands. Periscope depth is the depth at which a submarine interacts with the outside world. It has a periscope exposed along with one or more multi-purpose masts. During routine operations, a submarine is at periscope depth to conduct communications (receive and transmit), to establish navigational fixes, to perform housekeeping, and to ventilate the submarine atmosphere. During operations in shallow waters, the time spent at periscope depth will greatly

increase and may be the only depth the submarine is able to operate. As a result, the hydrodynamic influences on the submarine at periscope depth are of special interest.

This work primarily examines the free surface effects on submerged bodies similar to submarine hulls. As a submerged body travels through the water, it generates waves which interact with the free surface. This, in turn, produces forces and moments on the body. A longitudinal force, drag, opposes the body's motion, while a normal force, lift, pushes the body to the surface. Additionally, a moment is produced on the body which causes the body either to pitch up or down. Of these three effects, lift is the most important, since it's desirable to keep the body from breaking the free surface (broaching). Broaching hazards the submarine by making it much more susceptible to detection from air, sea or land sources. It is also desirable to minimize the moment in order that the stern (propeller) not break the free surface. A propeller out of the water greatly reduces the submarine's speed, making depth control much more difficult and also increases the submarine's detectability. Prior to proceeding to periscope depth, a submarine crew will adjust its trim by taking on additional weight (seawater) into forward, aft or auxiliary (middle) ballast tanks. This ballast will help counteract the upwards, sea-suction lift force encountered when operating near the free surface. However, taking on too much ballast makes it difficult to reach periscope depth and

could cause the submarine to lose depth control (sink out) once periscope depth is reached. Once at periscope depth, the ordered depth is maintained using a combination of speed, control surfaces (bow/fairwater planes, stern planes, and rudder) and variable ballast. These are used to prevent broaching and to keep the propeller submerged.

In addition to the waves the submerged body produces, the existing seas greatly effect the operation of the body near the surface. A submarine can easily maintain depth in calm seas, but in the presence of high sea states, depth control is much more difficult. The submarine pitches and rolls in the presence of sea waves and this reduces the crew's ability to keep the submarine submerged. The resulting drag, lift and moment from the incident waves are presented in this work. The results from the wave making and the incident wave problems can be linearly combined to produce a total effect on the submerged body.

On the practical side, the results of this work can be utilized in the simulation based design process as well as during training in submarine simulators. Additionally, they could be incorporated into future automatic depth control system designs. Also, incorporation into the existing SFMPL (Ship's Fleet Mission Program Library) would allow a submarine crew to make accurate predictions of the ballast required at periscope depth. The wave making and incident wave results are linearly added to the forces and moments produced by other

significant effects such as added mass from the body's acceleration, frictional resistance due to viscosity, and eddy resistance from appendages, to create a combined total force and moment acting on the body. The addition of these two effects due to operation near the free surface will greatly enhance the accuracy and realism of the simulators and improve future submarine designs.

For this work, the Defense Advanced Research Projects Agency (DARPA) SUBOFF model (DTRC Model 5470) (Roddy,1990) is utilized to provide the submerged hull shape into the computer program. The FORTRAN program written by Doctors and Beck calculates the drag, lift and moment coefficients for a given set of input conditions. For the wave making or Neumann-Kelvin problem, the free surface flow created by a moving submerged body is solved for (Doctors & Beck,1987). The program yields a solution to this problem, in which the fluid is inviscid and exact body boundary conditions (no normal velocity on the body surface) are satisfied. The sea surface condition is linearized, rather than being met exactly. The SUBOFF model is discretized into panels of constant source strengths using the method of Hess and Smith (Hess & Smith,1964 and Parsons,1984). The source strengths are then solved for such that the body boundary condition is satisfied. For the incident wave problem, the program uses a given expression for the pressure distribution, applies it to each

discrete hull panel and then sums the resulting forces and moment. This is examined for various depths, body speeds and wave directions.

In this work, the two problems are initially formulated in Chapter II. The inviscid flow theory development and an explanation of the boundary conditions explain the theoretical background needed to understand the wave making problem (Doctors & Beck,1987 and Papoulias,1993 and Papoulias & Beck,1988 and Reed & Beck & Griffin & Peltzer,1990). The incident wave problem is next set forth (Papoulias,1993) followed by a brief discussion on the numerical solution techniques. Chapter III presents the results. After determining the number of integration points needed for convergence, the results of the wave making and incident wave problems are presented. The wave making runs show the drag, lift and moment as a function of both speed and depth. The incident wave runs show these three parameters as a function of depth, body speed and wave direction for various wavelengths. After exploring the wave making and incident wave problems, Chapter IV presents a parametric study of submarine hull shapes. The submarine hull is described by three sections, a cylindrical parallel midbody with a parabola of revolution bow (entrance) and an ellipsoid of revolution stern (run) (Jackson,1992). The shape of the entrance and run can be varied by changing coefficients in the mathematical expression for each. Two effects are examined. In the first,

the displacement and the diameter are fixed and the length is varied. In the second case, the displacement and the length remain constant and the diameter is changed. In both cases, the drag, lift and moment are investigated for both the wave making and incident wave cases. These parametric studies have direct application in the design process of future classes of submarines. For a given set of requirements, the effect on lift and moment can be explored to provide an optimum solution to periscope depth operations. Thus, this work increases the understanding of near surface effects on a submerged submarine.

II. PROBLEM FORMULATION

A. INTRODUCTION

In the development of the free surface effects on submerged bodies, the forces and moments acting on the submerged body must calculated. The forces include the drag (force parallel to the body), the lift (force normal to the body) and the bow-up moment. These hydrodynamic forces acting on the submerged body arise from a modification to the pressure distribution summed around the surface area of the body in question. Forces can arise from relative motion velocity between the body and the fluid. This relative motion can be either time varying or time invariant. The approach utilized here considers only the time invariant cases of the motion of the body through a stationary fluid or the motion of the seaway relative to the body. Thus, the inertia forces from an accelerating body or from time varying seaways are neglected. This assumption simplifies the problem and is a first step towards a comprehensive modelling of a submarine at periscope depth.

In examining the combined effects of the relative motion between the body and the fluid, the system is considered to be a linear system and thus the principle of superposition applies. Separate effects can be examined independently and

the results summed together. This work considers two separate effects. The first, the wave making problem, is the motion of the body relative to a stationary fluid, resulting in forces and moments being generated on the body. The free surface is assumed to be an otherwise calm sea. Any modification in the free surface shape (waves) is due to the influence of the body itself. The second consideration is the effects of an existing seaway on the body or the incident wave problem. These two effects can then be summed together to yield the total response of both effects.

The appropriate fluid mechanics tools that are used to describe sea waves and ship motions are based on potential flow theory. The first fundamental assumption of ideal (potential) flow theory is that mass is preserved. If we consider a control volume surrounding the fluid and bodies of interest, what mass enters the volume either accumulates inside or leaves the control volume. This can be expressed mathematically by utilizing the divergence theorem: Given a closed surface area S with a unit vector $\bar{n}$ pointing inward, and volume V enclosed by S, then for any single valued and differentiable vector function $\bar{A}$,

$$\iint_S \bar{A} \cdot \bar{n} dS = - \iiint_V \nabla \cdot \bar{A} dV \quad . \tag{1}$$

If we denote the unit vector,

$$\bar{n} = n_x\hat{i} + n_y\hat{j} + n_z\hat{k} \quad , \tag{2}$$

then,

$$\bar{A}\cdot\bar{n} = A_x n_x + A_y n_y + A_z n_z \quad , \tag{3}$$

which is the component of $\bar{A}$ in the direction of $\bar{n}$. If we denote the operator,

$$\nabla = \frac{\partial}{\partial X}\hat{i} + \frac{\partial}{\partial Y}\hat{j} + \frac{\partial}{\partial z}\hat{k} \quad , \tag{4}$$

then the dot product,

$$\nabla\cdot\bar{A} = \frac{\partial A_x}{\partial x} + \frac{\partial A_y}{\partial y} + \frac{\partial A_z}{\partial z} \quad . \tag{5}$$

Conservation of mass then requires,

$$\frac{\partial}{\partial t}\iiint_V \rho\, dV = \iint_S \rho\bar{U}\cdot\bar{n}\, dS \quad , \tag{6}$$

where the right hand side represents the net mass flow in, and the left hand side the increase of mass in V. Applying the divergence theorem, we get,

$$\frac{\partial}{\partial t}\iiint_V \rho\, dV = -\iiint_V \nabla\cdot(\rho\bar{U})\, dV \quad , \tag{7}$$

and, since V is an arbitrary volume,

$$\frac{\partial \rho}{\partial t} + \nabla \cdot (\rho \bar{U}) = 0 \quad . \tag{8}$$

If we assume that the density ρ is constant, a good assumption in naval hydrodynamics, we get,

$$\nabla \cdot \bar{U} = 0 \quad . \tag{9}$$

If the velocity vector $\bar{U}$ is,

$$\bar{U} = u\hat{i} + v\hat{j} + w\hat{k} \quad , \tag{10}$$

we get the final form of the continuity equation,

$$\frac{\partial u}{\partial x} + \frac{\partial v}{\partial y} + \frac{\partial w}{\partial z} = 0 \quad , \tag{11}$$

inside the control volume V.

The next very important, and not so obvious, assumption is that the flow is irrotational (flow without rotation). One important property of irrotational flows is that the circulation around any closed curve c is zero,

$$\int_c \bar{U} \cdot d\bar{s} = 0 \quad . \tag{12}$$

This means that this line integral will be independent of the path of integration, which can only be achieved if $d\bar{s} \cdot \bar{U}$ is an

exact differential of some function ϕ,

$$d\phi = d\bar{s} \cdot \bar{U} \quad . \tag{13}$$

If we denote the position vector,

$$d\bar{s} = \hat{i}dx + \hat{j}dy + \hat{k}dz \quad , \tag{14}$$

we get,

$$d\bar{s} \cdot \bar{U} = udx + vdy + wdz = d\phi \quad . \tag{15}$$

Since the form of the total differential is,

$$d\phi = \frac{\partial \phi}{\partial x}dx + \frac{\partial \phi}{\partial y}dy + \frac{\partial \phi}{\partial z}dz \quad , \tag{16}$$

we get,

$$u = \frac{\partial \phi}{\partial x} = \phi_x \, , \quad v = \frac{\partial \phi}{\partial y} = \phi_y \, , \quad w = \frac{\partial \phi}{\partial z} = \phi_z \quad , \tag{17}$$

or, in vector form,

$$\bar{U} = \nabla \phi \quad , \tag{18}$$

which is the definition of the velocity potential. This is a very useful quantity since instead of computing the fluid velocity which is a vector function, $\bar{U}$, all we have to do is compute the scalar velocity potential ϕ, and then we can get

the components of $\bar{U}$ by differentiation. Using ϕ, we can write the continuity equation as follows,

$$\nabla \cdot \bar{U} = 0 \Rightarrow \nabla \cdot \nabla\phi = 0 \quad , \tag{19}$$

or,

$$\nabla^2\phi = \frac{\partial^2\phi}{\partial x^2} + \frac{\partial^2\phi}{\partial y^2} + \frac{\partial^2\phi}{\partial z^2} = \phi_{xx} + \phi_{yy} + \phi_{zz} = 0 \quad , \tag{20}$$

which is Laplace's equation.

This is the equation we have to solve, subject to appropriate boundary conditions, to compute the flow field of an ideal flow. Once we compute ϕ and the velocities, we can find pressure by using Bernoulli's equation,

$$p + \rho\frac{\partial\phi}{\partial t} + \frac{1}{2}\rho\nabla\phi \cdot \nabla\phi + \rho g z = c \quad , \tag{21}$$

where c is a constant, taken equal to zero in most cases. This form is similar to the usual form of Bernoulli's equation, $\nabla\phi \cdot \nabla\phi = U^2$ with the extra term $\partial\phi/\partial t$ due to the possible unsteady (always irrotational) nature of the flow. The pressure p can then be computed from,

$$p = -\rho\frac{\partial\phi}{\partial t} - \frac{1}{2}\rho\nabla\phi \cdot \nabla\phi - \rho g z \quad . \tag{22}$$

The first two terms represent the hydrodynamic contribution to the pressure and the third term represents the hydrostatic contribution. Integration of the pressure distribution then over the surface of the body will produce forces and moments.

To summarize, the basic features of potential flows are:

1. Mass is conserved and fluid density is constant. This results in,

$$\nabla \cdot \bar{U} = 0 \quad , \tag{23}$$

the continuity equation.

2. The flow is irrotational, which means we can define the velocity potential,

$$\bar{U} = \nabla \phi \quad , \tag{24}$$

which satisfies Laplace's equation,

$$\phi_{xx} + \phi_{yy} + \phi_{zz} = 0 \quad . \tag{25}$$

3. For unsteady, irrotational flows, we can use Bernoulli's equation,

$$p + \rho \frac{\partial \phi}{\partial t} + \frac{1}{2} \rho \nabla \phi \cdot \nabla \phi + \rho g z = 0 \quad . \tag{26}$$

This comes from Newton's law, and as such it is relative to an inertial coordinate system. It is noted here that throughout

the remainder of this work, partial derivatives will be designated by a subscript vice the $\partial/\partial x$ notation (i.e., ϕ_x vice $\partial\phi/\partial x$).

Wave effects on the free surface are important effects to consider on a submerged body. The most common and important wave phenomena are free surface waves that exhibit typical periods of a few seconds. Other waves like subsurface or internal waves are found in regions of density stratification beneath the free surface and are typically of lower frequency with periods on the order of several minutes. The influence of such waves on submerged bodies is generally negligible unless the body has an unusually low frequency resonance. The simplest free surface wave formation is the plane progressive wave system. This motion is two dimensional, sinusoidal in time with angular frequency, ω, and propagates with phase velocity, c_p, such that to an observer moving with this velocity the wave appears to be stationary. The waves could also be modelled as a series of random waves, where random refers to the character of the wave height distribution. These can be represented using a probabilistic approach. This work, however, views the waves as plane progressive waves of small amplitude, with sinusoidal time dependence. Effects of changing depth, varying wave period (and frequency) and altering wave direction are explored. Additionally, the interaction of the incident waves on the body, known as wave

diffraction, is neglected. This is a valid assumption since the incident wavelengths are the same magnitude as the body length and significant diffraction is not expected to occur.

B. WAVE MAKING PROBLEM

In the following, a right handed coordinate system is used with the origin at the projection onto the free-surface of the intersection of the horizontal centerline and midships. The positive x-axis points out the bow, the y-axis is positive to port and the z-axis in position upward. The submerged body is at a depth H below the undisturbed free surface and of diameter D at midships. Figure 1 illustrates this.

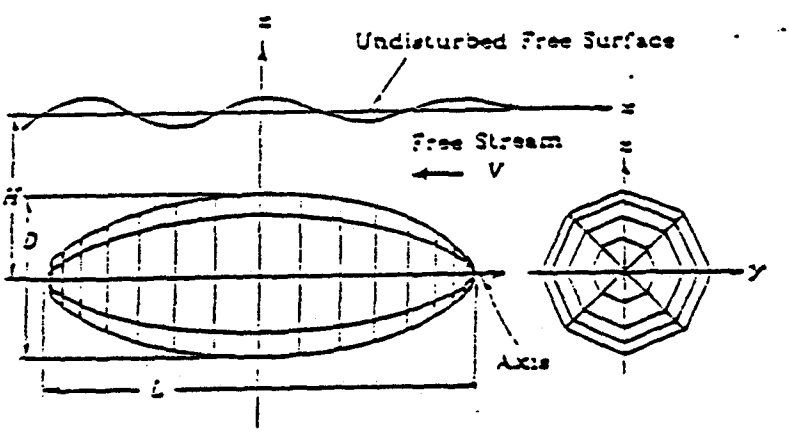

Figure 1: Definition of the Coordinate System

The total potential for a submerged body advancing with a constant speed U in an otherwise calm, inviscid and incompressible fluid is given by

$$\Phi(x,y,z) = -Ux + \phi(x,y,z) \quad , \tag{27}$$

where Φ is the free stream potential and ϕ is the perturbation potential due to the motion of the body alone. Assuming ϕ is small relative to Ux, the boundary value problem and its boundary condition may be rewritten in terms of ϕ. As such, ϕ satisfies the Laplace's equation

$$\nabla^2\phi = 0 \quad . \tag{28}$$

On the free surface, two boundary conditions apply. The first is the dynamic free-surface condition, which ensures constant pressure on the free surface. The wave elevation, $\eta(x,y)$, may be expanded in a Taylor series about z=0, where all higher order terms are neglected to obtain

$$g\eta + \frac{1}{2}\{(\Phi_x)^2 + (\Phi_y)^2 + (\Phi_z)^2\} = \frac{1}{2}U^2 \quad , \quad on \quad z = \eta(x,y) \tag{29}$$

where g is the acceleration due to gravity. The second is the kinematic free-surface boundary condition, which requires that there be no flow through the free-surface,

$$\Phi_x\eta_x + \Phi_y\eta_y - \Phi_z = 0 \quad , \quad on \quad z = \eta(x,y) \quad . \qquad (30)$$

Rewriting the dynamic, (29), and the kinematic, (30), free-surface conditions:

$$g\eta + \frac{1}{2}\{2U\phi_x + (\phi_x)^2 + (\phi_y)^2 + (\phi_z)^2\} = 0 \quad on \quad z = 0 \quad , (31)$$

and

$$U\eta_x + \phi_x\eta_x + \phi_y\eta_y - \phi_z = 0 \quad on \quad z=0 \quad . \qquad (32)$$

Neglecting the quadratic terms in both equations, and differentiating the dynamic free-surface condition with respect to x and subtracting the result from the kinematic conditions, gives the linearized free-surface condition:

$$\phi_{xx} + k_0\phi_z = 0 \quad on \quad z=0 \quad , \qquad (33)$$

where $k_0 = g/U^2$.

The boundary condition on the surface of the body, the body boundary condition, states that there shall be no flow through the surface of the body:

$$\frac{\partial\Phi}{\partial n} = 0 \quad , \quad on \quad f(x,y) - z = 0 \quad , \qquad (34)$$

where $\partial/\partial n$ denotes the derivative in the direction of the three dimensional normal vector pointing into the body ($\bar{n}$) and f(x,y) represents the surface of the body. This body boundary

condition can also be written as

$$\frac{\partial \phi}{\partial n} = \bar{U} \cdot \bar{n} = - U \frac{f_x}{\sqrt{1 + (f_x)^2 + (f_y)^2}} \quad , \quad on \quad f(x,y) - z = 0 \quad . \tag{35}$$

A fundamental solution of (28) and (33) is the Green function, given by

$$G(P,Q) = \frac{1}{r} - \frac{1}{r'} + \breve{G}(P,Q) \quad , \tag{36}$$

where

$$\breve{G}(P,Q) = \frac{k_0}{\pi} \underset{\mu \to 0}{Lim} \int_{-\pi}^{\pi} d\theta \int_0^{\infty} dk \frac{\exp\{k[z+\zeta+i(x-\xi)\cos\theta+i(y-\eta)\sin\theta]\}}{k_0 - k\cos^2\theta - i\mu\cos\theta} \tag{37}$$

where P = (x,y,z) is the field point, Q = (ξ, η, ζ) is a point source of strength -4π on the body , and

$$r, r' = [(x-\xi)^2 + (y-\eta)^2 + (z \mp \zeta)^2]^{1/2} \quad . \tag{38}$$

In this definition, r is the distance between the field point and the singularity point and r′ is the distance between the field point and the image of the singularity point in the

free-surface. The denominator of the integrand in (37) contains the Rayleigh virtual viscosity μ, which is taken to be small and positive, thus ensuring that the radiation condition is satisfied. The 1/r terms in (36) represent source and sink distributions typical in potential flow problems. The extra term,(37), represents a series of waves such that the free surface boundary condition (33) is automatically satisfied, where θ is the wave direction and k is the wavenumber. Finally, the radiation condition (i.e., all waves far away from the body are outgoing) is satisfied by taking μ to be positive. The only condition that still needs to be satisfied is the body boundary condition (35).

In the usual method of potential theory, Green's theorem can be applied to a large volume of fluid containing the body, and extending to infinity both laterally and in depth. The following result for the perturbation potential in terms of a pure source strength, σ, is obtained:

$$\phi(P) = -\frac{1}{4\pi}\iint_{S_H} G(P,Q)\,\sigma(Q)\,dS(Q) \quad , \qquad (39)$$

where S_H is the wetted surface of the body.

An integral equation for the source strength may be found by differentiating (39) with respect to the normal on the body and setting it equal to the body boundary condition which

requires that the normal velocity on the hull be zero. Using (27) and (39), we may write

$$Un_x = -\frac{1}{2}\sigma - \frac{1}{4\pi}\iint_{S_B} G_n(P,Q)\,\sigma(Q)\,dS(Q) \quad . \qquad (40)$$

Solution of (40) is achieved by discretizing the surface of the body into plane quadrilateral panels using the method of Hess and Smith, as described later. The equations are then assembled to yield a system of linear algebraic equations in terms of the unknown source σ. This method of solution is also known as the Neumann-Kelvin method. The flow past a body moving at a steady speed requires the body boundary condition be satisfied exactly, while the free-surface condition is satisfied in a linearized sense.

C. INCIDENT WAVES PROBLEM

A second major effect on a submerged body operating near the free surface is that of incident waves disturbing the otherwise calm free surface and interacting with the body. In the case examined in this work, the waves incident upon the body are two dimensional plane progressive waves of small amplitude, with sinusoidal time dependence. The wave motion is parallel to the x-z plane, with angular frequency ω, propagating with phase velocity c_p. The body motions are assumed to be sufficiently small so that linear theory holds.

The free surface elevation is of the general form

$$\eta(x,t) = A\cos(kx - \omega t) \quad , \tag{41}$$

where the positive x-axis is chosen to coincide with the direction of wave propagation. Here A is the wave amplitude, and the parameter $k = \omega/c_p$, is the wavenumber, the number of waves per unit distance along the x-axis. Clearly $k = 2\pi/\lambda$, where the wavelength λ is the distance between successive points on the wave with the same phase.

The solution of this problem is expressed in terms of a two dimensional velocity potential $\phi(x,z,t)$ which must satisfy Laplace's equation

$$\nabla^2\phi = 0 \quad , \tag{42}$$

and appropriate boundary conditions. Furthermore, ϕ must yield the wave elevation (41) from

$$\eta = -\frac{1}{g}\cdot\phi_t \quad . \tag{43}$$

Equation (43) is the so called linearized dynamic boundary condition on the free surface and is an expression of the fact, through Bernoulli's equation, that the pressure on the free surface must be the same as the ambient atmospheric pressure.

An appropriate boundary condition on the sea bottom is

$$\phi_z = 0 \quad , \quad at \quad z = -h \quad , \tag{44}$$

i.e., the bottom at depth h is a rigid impermeable plane. Finally, the free surface boundary condition is

$$\phi_{tt} + g\phi_z = 0 \quad , \quad on \quad z = 0 \quad . \tag{45}$$

Equation (45) is a combined dynamic and kinematic free surface boundary condition. The dynamic condition was mentioned before, while the kinematic condition simply states

$$\eta_t = \phi_z \quad , \tag{46}$$

i.e., the vertical velocities of the free surface and fluid particles are the same. Combining (43) and (46) we arrive at (45), ignoring the small departures of the free surface η from the horizontal orientation z = 0.

Clearly the velocity potential ϕ must be sinusoidal in the same sense as (41); therefore we seek a solution of the form

$$\phi(x,z,t) = \Re\{Z(z)\, e^{-ikx+i\omega t}\} \quad . \tag{47}$$

Substituting (47) into (42), Z must satisfy the ordinary differential equation

$$Z_{zz} - k^2 Z = 0 \quad , \tag{48}$$

throughout the domain of the fluid. The most general solution of (48) is given in terms of exponential functions in the form

$$Z = Ce^{kz} + De^{-kz} \quad . \tag{49}$$

Assuming infinite water depth (deep water), the constant D in (49) must be zero to avoid an unbounded motion deep beneath the free surface, resulting in

$$Z = Ce^{kz} \quad , \tag{50}$$

Substituting into (47)

$$\phi = \Re\{Ce^{kz-ikx+i\omega t}\} \quad . \tag{51}$$

Now substituting (51) into (43) with z = 0, and comparing the result with (41) we can find

$$C = \frac{igA}{\omega} \quad , \tag{52}$$

and

$$\phi = \frac{gA}{\omega} e^{kz} \sin(kx - \omega t) \quad . \tag{53}$$

An additional relation between the wavenumber k and the frequency ω can be obtained by substituting (53) into (45). This relation, called a dispersion relation is

$$k = \frac{\omega^2}{g} \quad . \tag{54}$$

The frequency ω can be replaced by the wave period $T = 2\pi/\omega$, just as k can be replaced by the wavelength $\lambda = 2\pi/k$.

The phase velocity c_p can be determined from the definition of the wavenumber and (54) to yield

$$c_p = \frac{\omega}{k} = \frac{g}{\omega} = \sqrt{\frac{g}{k}} = \sqrt{\frac{g\lambda}{2\pi}} \quad . \tag{55}$$

Equation (55) states that surface waves in deep water are dispersive; longer waves travel faster than shorter waves.

While the wave moves with the phase velocity c_p, the fluid itself moves with a much smaller velocity given by the gradient of the potential (53). The velocity components (u,w) of the fluid are

$$u = \phi_x = \omega A e^{kz} \cos(kx - \omega t) \quad , \tag{56}$$

$$w = \phi_z = \omega A e^{kz} \sin(kx - \omega t) \quad . \tag{57}$$

Within linear theory, the fluid particles move in small circular orbits proportional to the wave amplitude; they remain in the same mean position as the wave propagates through the fluid with a phase velocity independent of the wave amplitude. As the depth of submergence beneath the free surface increases, the fluid velocities (56) and (57) are attenuated exponentially. For a submergence of half a wavelength, $kz = -\pi$, the exponential factor is reduced to 0.04. Thus, waves in deep water are confined to a relatively shallow layer near the free surface, with negligible motion beneath a depth of about 0.5λ. On this basis one can anticipate that if the fluid depth is finite, but greater than half a wavelength, the effects of the bottom will be negligible.

For a fluid at constant depth h, the boundary condition (44) is imposed. Returning to the general solution (49), both exponential functions are retained, with the constants C and D suitably chosen to satisfy (44). In this case, the velocity potential (53) becomes

$$\phi = \frac{gA}{\omega} \frac{\cosh k(z + h)}{\cosh kh} \sin(kx - \omega t) \quad , \tag{58}$$

and the dispersion relation (54) is now

$$k \tanh(kh) = \frac{\omega^2}{g} \quad , \tag{59}$$

where we can see that as $h \to \infty$ we get the previous deep water results. The fluid velocity components can be computed as in (56) and (57), and for finite depth it follows that

$$u = \phi_x = \frac{gAk}{\omega} \frac{\cosh k(z + h)}{\cosh kh} \cos(kx - \omega t) \quad , \tag{60}$$

$$w = \phi_z = \frac{gAk}{\omega} \frac{\sinh k(z + h)}{\cosh kh} \sin(kx - \omega t) \quad . \tag{61}$$

In this case the fluid particle trajectories are elliptical, with the major axis being horizontal.

The phase velocity for finite depth can be expressed in the form

$$c_p = \frac{\omega}{k} = \sqrt{\frac{g}{k} \tanh kh} \quad . \tag{62}$$

This tends to the deep water limit (55) for $kh \gg 1$. The opposite limit, where $kh \ll 1$, is the regime of shallow water waves. In this case (62) can be approximated using the Taylor series expansion for the hyperbolic tangent, and the leading order approximation for the phase velocity is

$$c_p = \sqrt{gh} \quad , \quad for \quad kh \ll 1 \quad . \tag{63}$$

In the shallow limit, the resulting wave motion is nondispersive, since the phase velocity depends only on the depth.

Once the velocity potential is determined we can obtain the total pressure by substitution into Bernoulli's Equation (22) which is repeated here

$$p = -\rho\phi_t - \frac{1}{2}\rho\nabla\phi\cdot\nabla\phi - \rho gz \quad . \tag{64}$$

Using the deep water expression for the velocity potential ϕ (53) and solving (64) results in

$$p = -\rho gAe^{kz}\cos(kx - \omega t) - \frac{1}{2}\rho\omega^2A^2e^{2kz} - \rho gz \quad . \tag{65}$$

The first term in (65) is the time rate of change of the velocity potential and is neglected in this work since only time invariant effects are considered. The second term in (65) is the key element examined in this work. It represents the time invariant effect on the body and is the major contributor to the sea-suction forces on the body. The last term in (65) is the hydrostatic component of the total pressure and is likewise neglected. As before, the pressure is integrated over the entire surface to yield the resulting forces and moments.

The previous equations of motion are valid for a body with zero forward speed. If the body possesses a forward speed U, this can be assumed, within linearity, constant. The only change in such a case is in the frequency ω due to a Doppler shift effect. If we consider the case of head seas, or waves from directly ahead, we can assume that both the wave excitation forces and the resultant oscillatory motions are linear and harmonic, acting at the frequency of wave encounter

$$\omega_e = \omega + \frac{2\pi}{\lambda/U} = \omega + kU = \omega + \frac{\omega^2}{g}U \quad . \tag{66}$$

To account for the more general cases of waves at a direction θ, where $\theta = 180°$ corresponds to head seas and $\theta = 0°$ to following seas, the frequency of encounter ω_e becomes

$$\omega_e = \omega - \frac{\omega^2}{g}U\cos\theta = \omega - kU\cos\theta \quad . \tag{67}$$

The frequency of encounter and wave direction are utilized in this work to determine the incident waves effect on the submerged body. It should be emphasized that the mean second-order forces acting on a near surface submarine in a seaway are due entirely to time-averaged products of first-order quantities at each separate frequency of monochromatic wave encounter. In general these mean forces involve quadratic products of the radiation and diffraction potentials. The former is usually neglected (Bingham & Korsmeyer &

Newman,1994), which corresponds to the case where the submarine's unsteady motions are neglected.

Thus, the mean second order force can be written as

$$\bar{F}(\omega) = -\frac{1}{2}\rho \iint_S dS\, \bar{n}\, \overline{\nabla(\phi_I + \phi_S) \cdot \nabla(\phi_I + \phi_S)} \quad . \qquad (68)$$

Here the total diffraction potential $(\phi_I + \phi_S)$ is for a steady-state (regular wave) solution at a specified frequency of encounter, the overbar denotes the time average of one period, and $\bar{n}$ is the unit normal to the surface. In this work we neglect the effects of the scattering potential ϕ_S, and we consider only the incident waves potential ϕ_I. This is a good approximation for mostly head or following seas. For beam seas, the potential ϕ_S is expected to play an increasingly important role. It should be mentioned, however, that periscope depth operations in beam seas are not very common due excessive first-order roll motions.

D. NUMERICAL SOLUTION

Once the velocity potential for a distribution of sources is formulated, the source strengths can be solved for by satisfying the body boundary condition. There are various analytical techniques for doing this. This work utilizes the source panel method developed by Hess and Smith (Hess & Smith, 1964). Their method is detailed below.

The velocity potential was derived and given in (39) and repeated here

$$\phi(P) = -\frac{1}{4\pi}\iint_{S_H} G(P,Q)\,\sigma(Q)\,dS(Q) \quad , \tag{69}$$

where P(x,y,z) is the field or observation point and $Q(\xi,\eta,\zeta)$ is the distributed source point on the body surface. We must determine $\sigma(Q)$ to satisfy the body boundary condition on S_H. The surface is represented as a finite number of elements each having $\sigma(Q)$ constant so that the source strength can be brought outside of the integral. The integral then depends only on the geometry of the various panels. With a finite number of unknowns we can only satisfy the body boundary condition at an equal number of discrete points.

To form the panels the body surface is divided into N plane quadrilaterals with a constant σ_j source strength over each quadrilateral for j = 1,2,...N. The σ_j can then be moved outside the integral in (68) yielding the following formula for the perturbation potential

$$\phi(P) = \sum_{j=1}^{N} \sigma_j\left(-\frac{1}{4\pi}\right)\iint_{S_{H_j}} G(P,Q_j)\,dS_j \quad , \tag{70}$$

where $Q_j = (\xi_j,\eta_j,\zeta_j)$ is the source point at the j^{th} panel and dS_j is the surface area of the j^{th} panel. The integral can

then be obtained algebraically in terms of x,y,z and the four corners ξ_l, η_l, ζ_l for l = 1,2,3,4. If (x,y,z) is far from the panel, simplification can be used since the distance between the source point and the observation point is essentially constant over the whole panel. The body boundary conditions are applied at one point in each quadrilateral to form N linear equations in N unknowns which can then be solved for σ_j. Once the source strengths σ_j are determined, the velocities at the control points are computed from the formula

$$U_i = -\hat{i}U + \sum_{j=1}^{N} \nabla G_{ij}\sigma_j \quad , \tag{71}$$

where ∇G_{ij} is the gradient of the total Green function. This includes the effect of all three terms of (36) as well as both sides of the body. The Bernoulli Equation is then used to give the dynamic pressure

$$p_i = \frac{1}{2}\rho(U^2 - U_i^2) \quad . \tag{72}$$

The hydrostatic pressure is ignored.

In practice the Hess and Smith program works in a two-step process. The first step is the quadrilateral generation. Points are input which specify the body surface. The program then forms quadrilaterals as flat surfaces and determines the normal to that surface. It then finds the null point, this

being the point where the source of the panel produces no tangential velocity. Finally, it provides an output to check the points. The second step yields the solution. The program satisfies the body boundary condition at the null point of each quadrilateral to form N equations. It then solves for velocity and pressure at each null point for an inputted inflow in x, y, and z. Additionally, it will also obtain velocity and pressure at specified off the body. With the pressure at each panel known, the drag, lift and bow-up moments can be calculated by integrating over the appropriate areas and distances.

III. RESULTS

A. INTRODUCTION

To implement the Hess and Smith source panel method, a FORTRAN program written by Doctors and Beck provided the solution for all problem runs. This program computes the hydrodynamic forces and moments for a body travelling at a constant speed by the Neumann-Kelvin method. The key inputs to the program, stored in a file IN.DAT, included the following: water density, acceleration due to gravity, body length, body beam, body depth, body speed, and the number of points longitudinally, vertically and in the θ-integration. Parameters could be varied for particular runs. Additionally, the body surface was input with a data file of longitudinal points, with a corresponding radius at each point. A subroutine then calculated the y and z points from the radius (R) using the following relations:

$$y = R \sin(\pi(IZ - 1.0)/(NZ - 1.0)) \tag{73}$$

and

$$z = R \cos(\pi(IZ - 1.0)/(NZ - 1.0)) - H \quad , \tag{74}$$

where NZ is the total number of vertical points, IZ is the

successive vertical point and H is the depth. This scheme forms half of the body surface. The other half is formed by reflecting the points about the vertical centerline in a subroutine. The program then utilizes these points to generate the quadrilateral panels. Thus, the Doctors and Beck program provides the numerical solution to the Neumann-Kelvin problem for numerous inputs.

The output results, stored in a file OUT.DAT, contained appropriate body parameters as well as the three primary coefficients. The program calculated the drag and lift forces and bow-up moments by pressure summation over the body surface panels. The moments are referenced to the body midpoint. For the wave making problem, the drag coefficient, C_D, and the lift coefficient, C_L, were made dimensionless by $1/2\rho U^2 S$, where S = wetted area, ρ = water density and U = body speed. The bow-up moment coefficient, C_M, was made dimensionless by $1/2\rho U^2 SL$, where L = body length. For the incident waves problem, the forces and moment were nondimensionalized using $1/2\rho A^2\omega^2 S$ and $1/2\rho A^2\omega^2 SL$, respectively. Here A = wave amplitude and ω = wave frequency. These nondimensional coefficients served as the basis for evaluating the effects on the body.

The model used to generate the input data points was a submarine model, SUBOFF. Developed by the Defense Advanced Research Projects Agency (DARPA), the model was originally developed to evaluate various flow field predictions for an

axisymmetric hull, both with and without appendages. It was intended to compare predictions with model experimental data. For all runs in this work, data for a bare hull (no appendages) model were utilized. The key parameters of this model are a length of 14.2917 ft, a 1.6667 ft midbody diameter and a displacement of 24.692 ft^3. To model the hull surface, various station points (longitudinal points) were provided along with their corresponding radius (fraction of midbody diameter). These points are tabulated in Table I. These station points were converted into corresponding x values, with station 0.0000 at the bow (+L/2) and station 20.4167 at the stern (-L/2). The radius values were used to produce the y and z values. A drawing of the DARPA SUBOFF model is included as Figure 2. The remaining sections of this chapter detail the convergence, the wave making problem and the incident waves problem results. The convergence section explores the optimum number of vertical and θ steps required to converge to an acceptable solution. The wave making problem section examines the depth dependence of each coefficient over a range of speeds. Finally, the incident waves section looks at two areas. The first is the effect on the coefficients when the wave period is varied. The second area shows the effect on the coefficients when the wave frequency of encounter and the wave direction is altered.

TABLE I. SUBOFF STATION POINTS AND RADII

STATION POINTS	RADIUS FRACTION
0.0	0.00000
0.1	0.29058
0.2	0.39396
0.3	0.46600
0.4	0.52147
0.5	0.56627
0.6	0.60352
0.7	0.63514
1.0	0.70744
2.0	0.84713
3.0	0.94066
4.0	0.99282
7.7143	1.00000
10.0	1.00000
15.1429	1.00000
16.0	0.97598
17.0	0.81910
18.0	0.55025
19.0	0.26835
20.0	0.11724
20.1	0.11243
20.2	0.10074
20.3	0.07920
20.4	0.03178
20.4167	0.00000

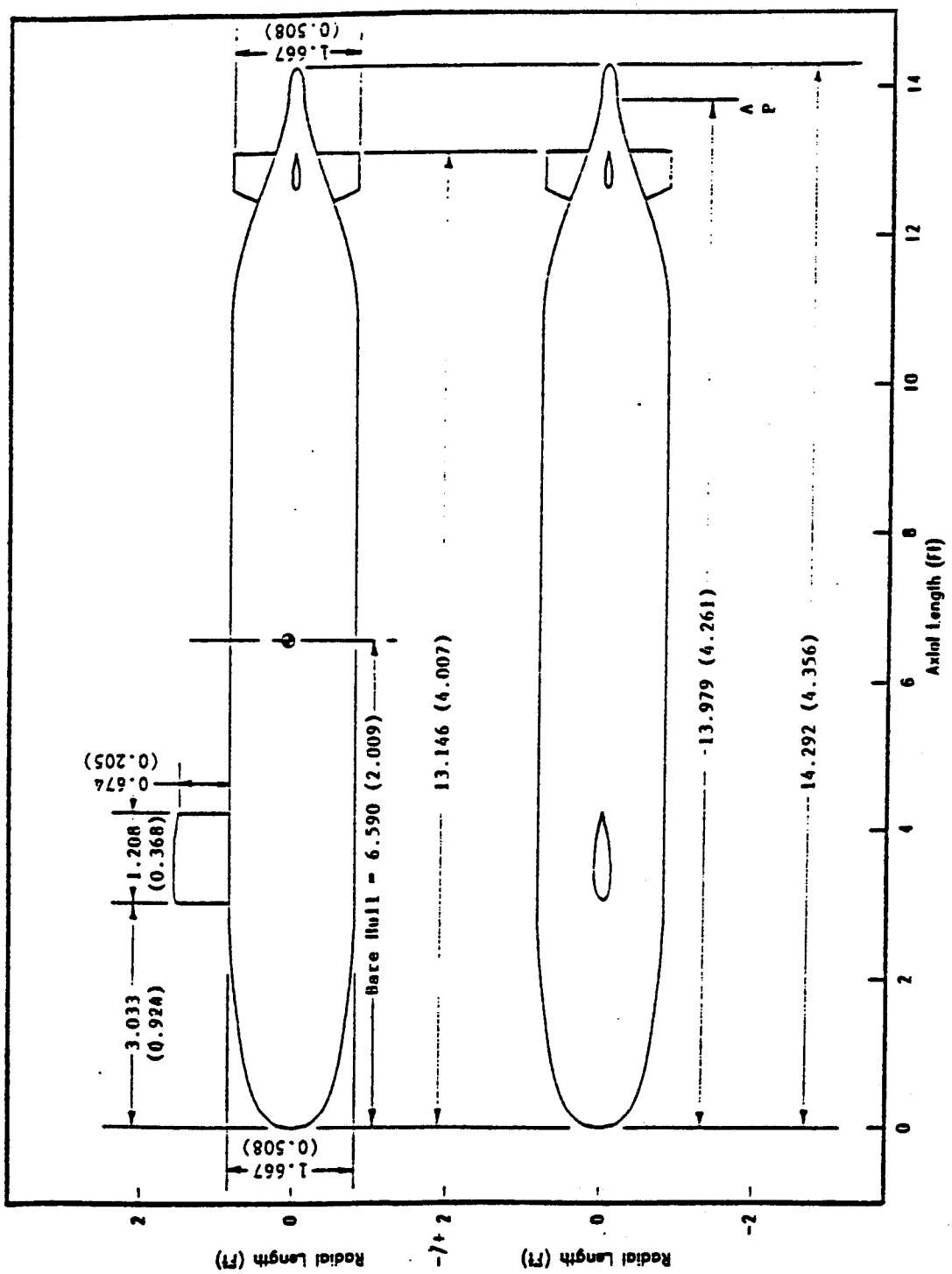

Figure 2: Drawing of the DARPA SUBOFF

B. CONVERGENCE

The first step in producing accurate results requires a consistent number of integration increments in the vertical and θ-directions be used for each run. The longitudinal or x increments (NX) are fixed by the station points of the DARPA SUBOFF model at 25. A series of computer runs, using standard input data, was conducted to determine the number of vertical steps, NZ, and the number of θ-steps, Nθ. The input conditions were standardized as follows:

- ρ = 1.94 slugs/ft^3
- g = 32.2 ft/sec^2
- L = 14.3 ft
- D = 1.67 ft
- H = 0.15L = 2.15 ft
- U = 10.0 ft/sec
- NX = 25

The convergence for the θ-steps (Nθ) was first conducted. The depth-to-submergence ratio, H/L, of 0.15 was chosen to closely correspond to the value of 0.16 that Doctors and Beck utilized in their study of a submerged spheroid. The spheroid had a depth-to-length ratio of 0.2, whereas the SUBOFF has a ratio of 0.12. Five runs were conducted, using a fixed value of vertical steps, NZ = 8. The runs varied NH from 4 to 20, in increments of 4. Figures 3 to 5 clearly show a large change in all three coefficients for values of NH below 8.

Comparing the percent change between Nθ = 4 and Nθ = 8 for each plot, the drag coefficient (C_D) varied by only 0.80%, the lift coefficient (C_L) changed by 11.9% and the moment coefficient (C_M) rose by 1.44%. Above Nθ = 8, the plots show a nearly constant value. C_M steadied at -2.76E-2, C_L leveled at 1.51E-3 and C_D stabilized at 7.84E-3. Since a value of Nθ = 16 yielded effectively convergent results for each coefficient (to three significant figures), this value was chosen as the standard for all subsequent runs. This selection was important, as the computational time varied with the square of Nθ.

To study the effects of the vertical steps, NZ, the value of Nθ was fixed at 16. NZ was varied from 4 to 9 in steps of one. Figures 6 through 8 show the convergence plots. In each case, the plot has not leveled off at NZ = 9. However, the slope in each plot has significantly decreased by NZ = 8 from its initial value at NZ = 4. Drag slope dropped from 8.47E-4 to 1.14E-4, lift slope changed from 2.25E-4 to 3.03E-5, and moment slope varied from -2.99E-4 to -3.11E-5. Between NZ = 8 and NZ = 9, the values of the drag, lift and moment coefficients vary by only 1.45%, 2.00%, and 1.13%, respectively. A value of NZ = 8 was chosen as the standard for future runs based on this reasonable convergence. Choosing more vertical points would not significantly improve the solution. Additionally, it would also increase the computational time since it is also proportional to the square

of the number of panels. Also, the ratio of NX/NZ = 25/8 = 3.125 is smaller than the ratio of 4 used in the Doctors and Beck study to achieve reasonable convergence. The smaller ratio is better since the quadrilaterals that are formed will have a more uniform shape than a body with a higher aspect ratio.

Values of Nθ = 16 and NZ = 8 were selected as the standards for subsequent runs. As this section detailed, these values give good convergence results in reasonable computational time. Using these values, the runs to determine the wave making effects of the body, were performed.

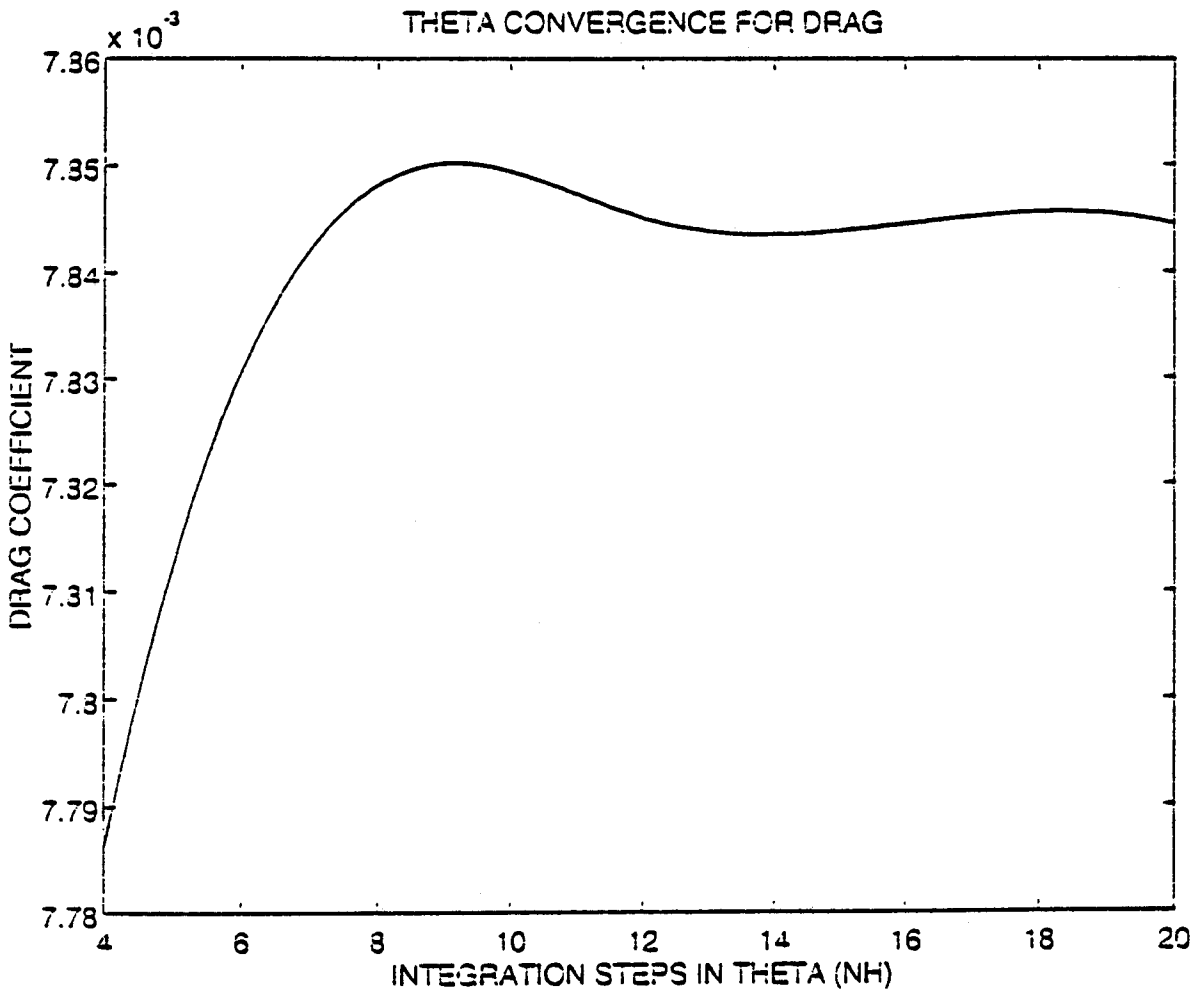

Figure 3: Theta Convergence for Drag Coefficient

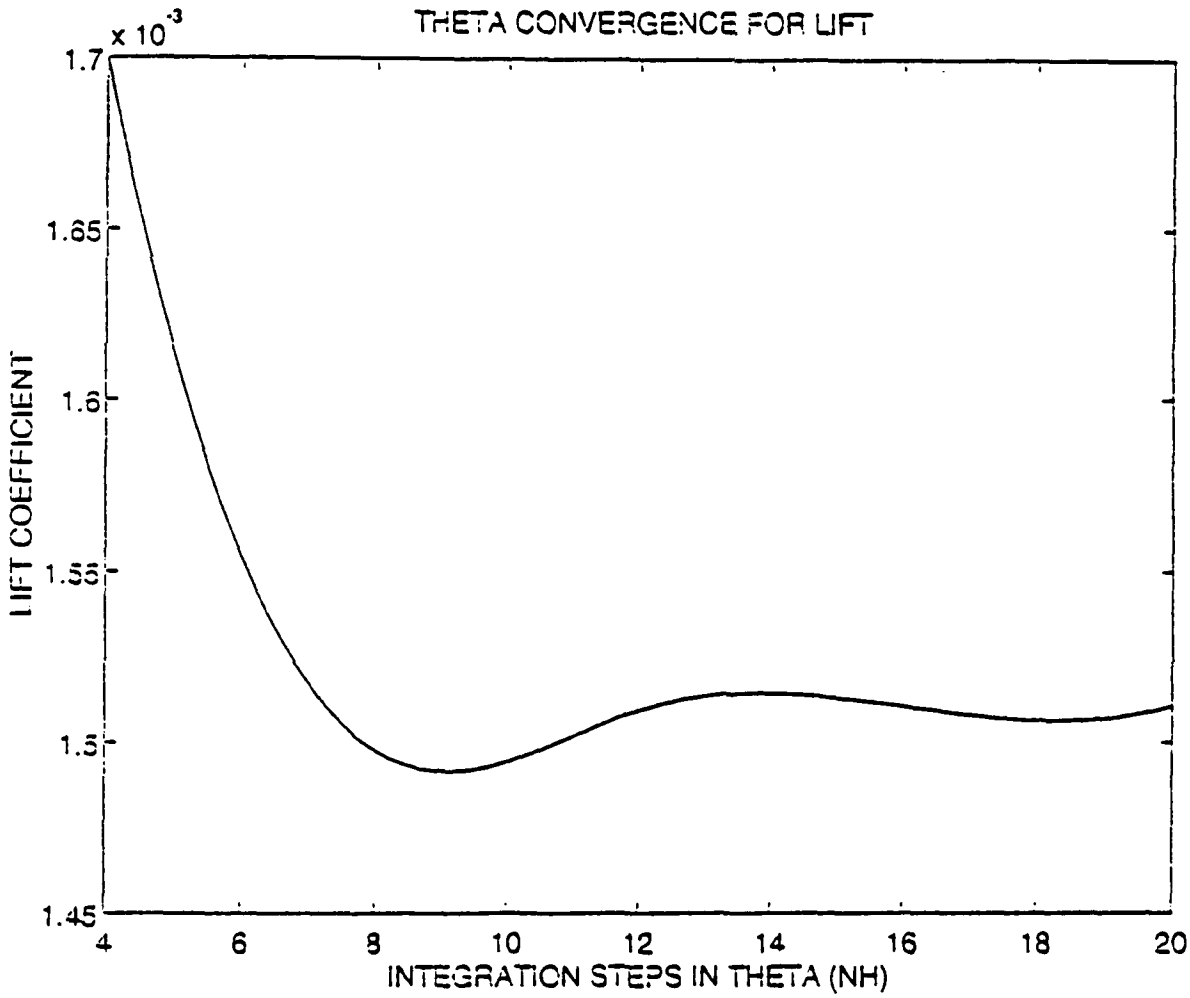

Figure 4: Theta Convergence for Lift Coefficient

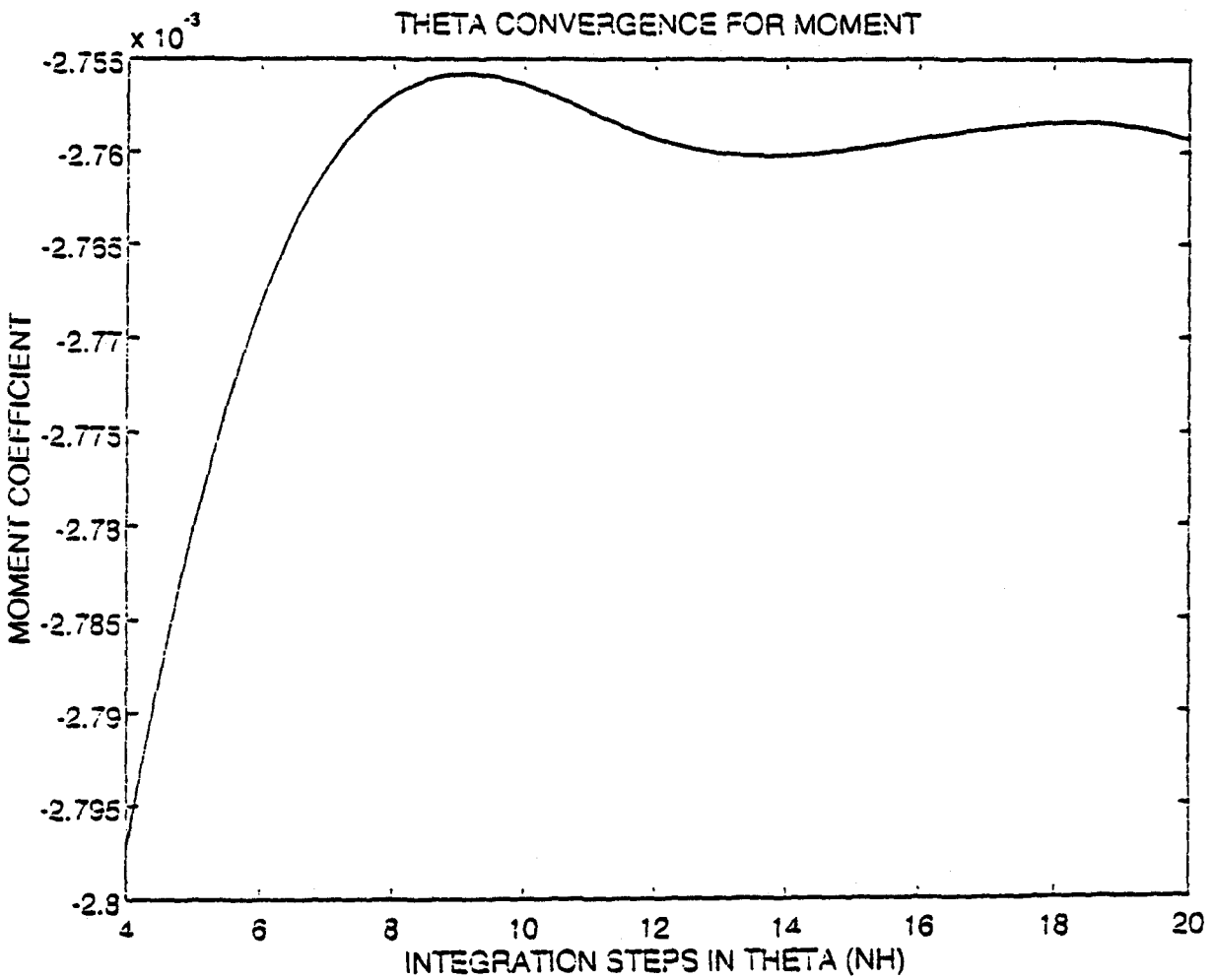

Figure 5: Theta Convergence for Moment Coefficient

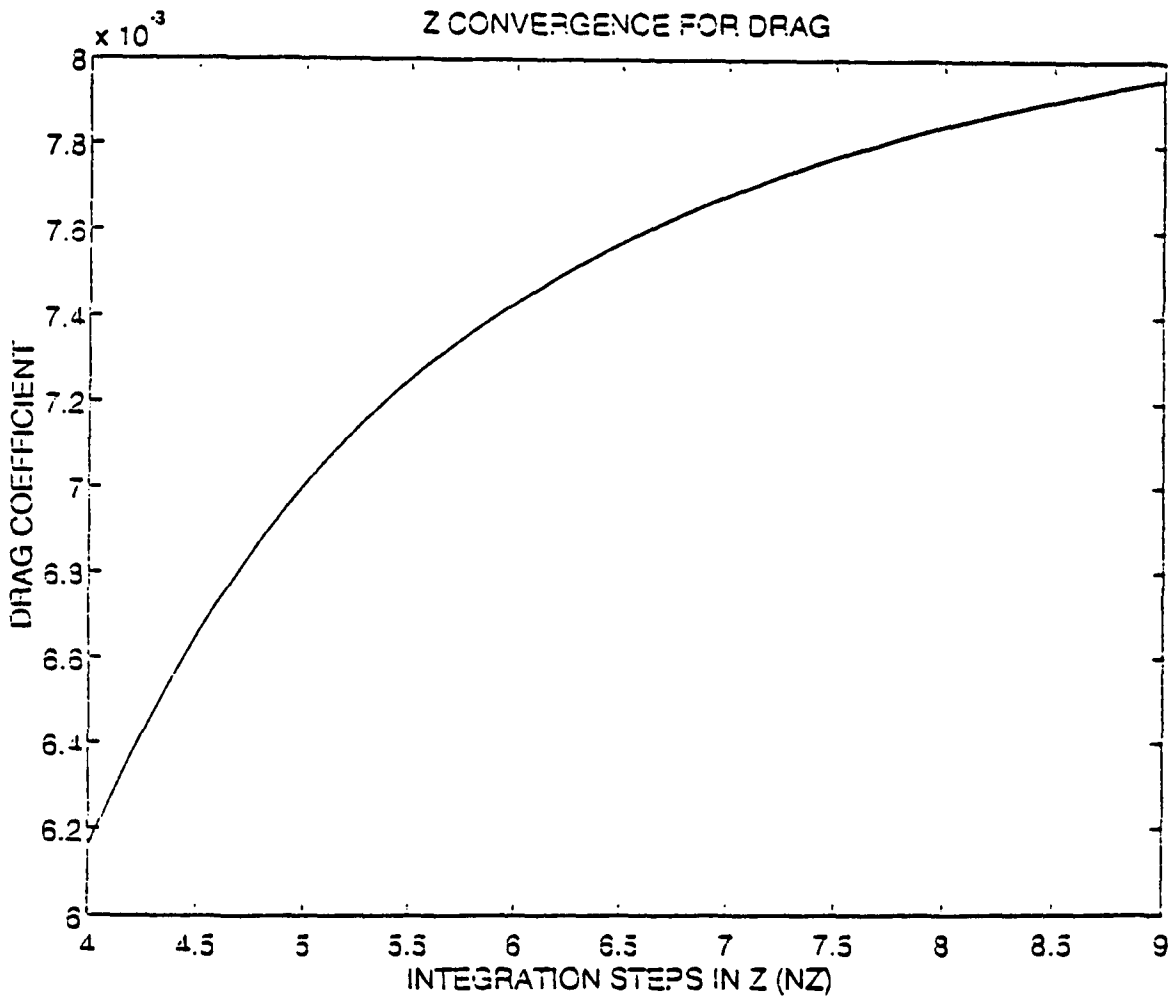

Figure 6: Z Convergence for Drag Coefficient

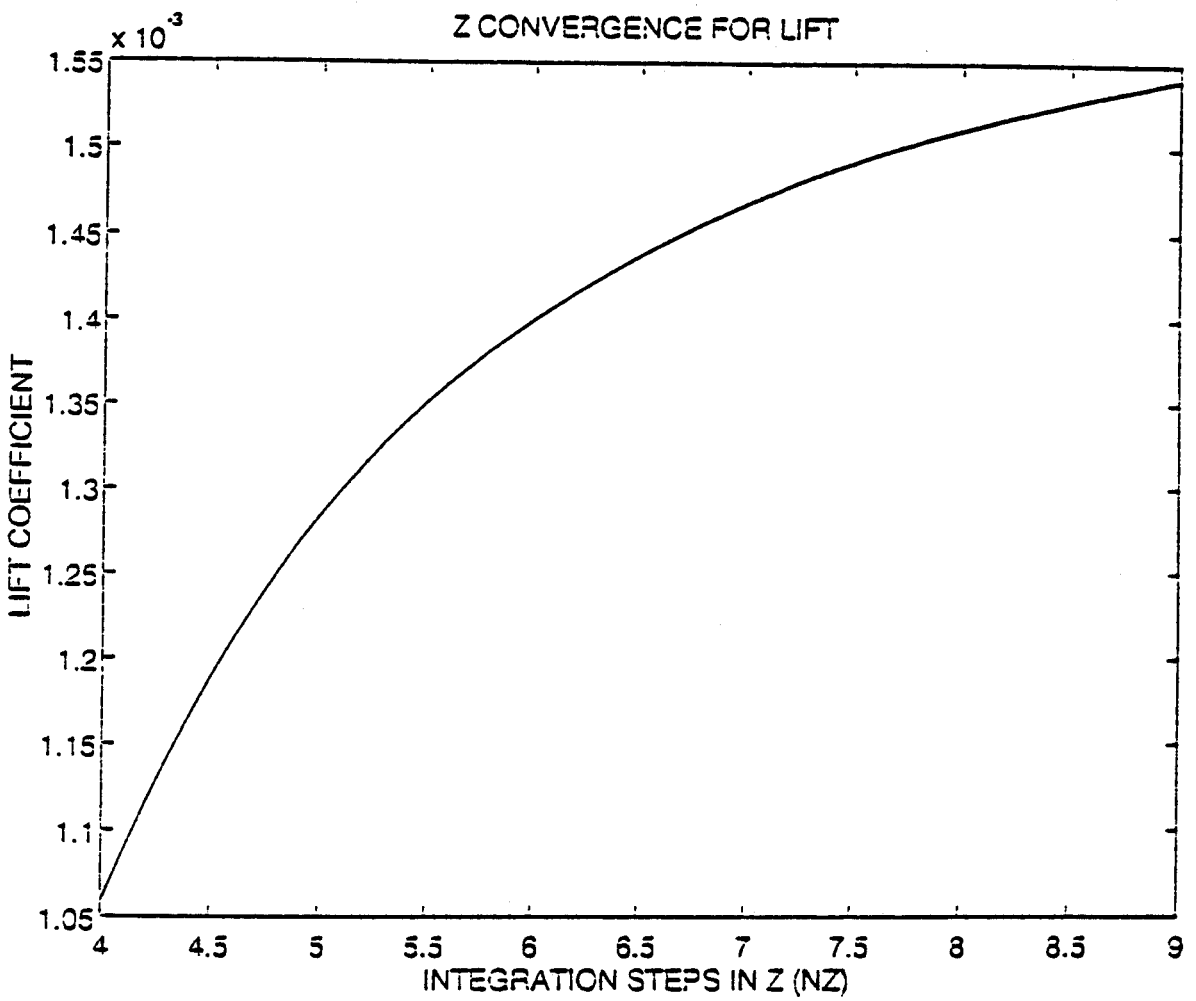

Figure 7: Z Convergence for Lift Coefficient

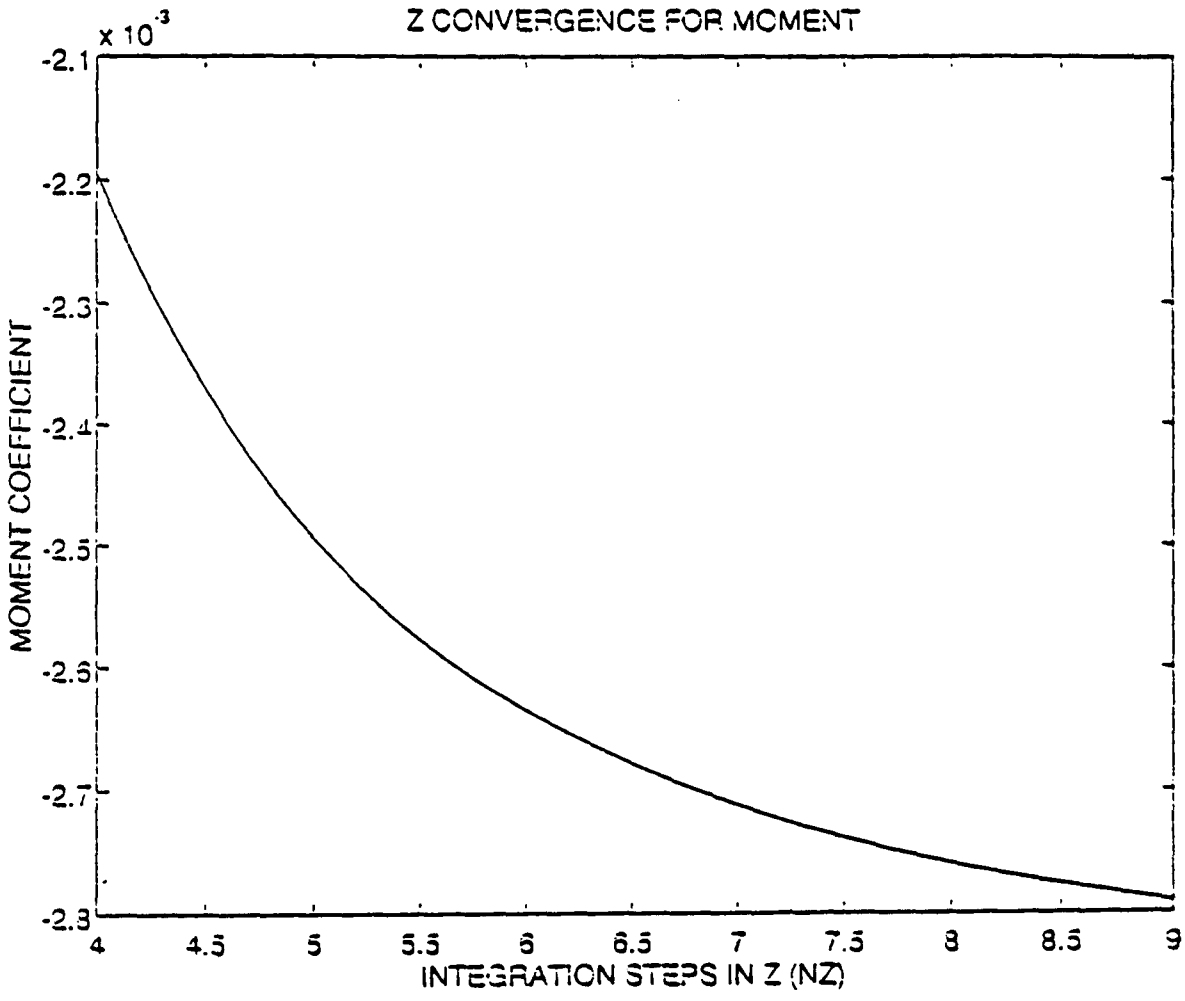

Figure 8: Z Convergence for Moment Coefficient

C. WAVE MAKING PROBLEM

Having established Nθ and NZ, the DARPA SUBOFF model is input into the program to solve the wave making problem. The drag, lift and moment coefficients are calculated as a function of the body speed (Froude number) for varying depths. The Froude number is

$$F = \sqrt{\frac{U^2}{gL}} \quad , \tag{75}$$

where U is the body speed in ft/sec, g is the acceleration due to gravity and L is the body length. The depths (H) were chosen to be a fraction of the ship length, ranging from one tenth to one half. The following depth ratios (H/L) were chosen to give a good spread of values, with more runs performed at shallower depths:

- 0.100
- 0.110
- 0.120
- 0.125
- 0.135
- 0.150
- 0.175
- 0.200
- 0.225

- 0.250
- 0.300
- 0.400
- 0.500

Figures 9, 10, and 11, plot the drag, lift and moment coefficients versus Froude number. The shallowest (0.1) and the deepest (0.5) depth ratios are labelled, with each successive curve being the sequential plot from the above list. The Froude number is plotted from 0.18 to 0.75 which corresponds to a range of 4 to 16 ft/sec. A spline technique was utilized to smooth the curve.

The first plot, Figure 9, graphs the Drag Coefficient versus Froude Number. The drag coefficient indicates the force which is opposing the body in the longitudinal direction. The oscillatory nature of the curves is readily apparent especially at the shallower depths. At deeper depths, the near surface effects are greatly diminished and it exhibits small oscillations about a steady value of about 0.005. Two peaks are clearly seen at about F = 0.3 and F = 0.5. The magnitude of the peaks decreases and the peak shifts to the right as depth is increased. With the exception of the shallowest depth, the second peak (higher speeds) is of a greater magnitude than the first peak. For the shallowest depth, the ratio of the highest to lowest coefficient is about 3. This ratio drops off to just over 1 for the deepest depth.

Also noteworthy is the observation that at F = 0.2 and F = 0.35, a minimum coefficient is reached, regardless of depth. Clearly, the drag coefficient markedly decreases with depth, since the interaction with the calm free surface exponentially decays.

A similar oscillatory behavior is observed in Figure 10, Lift Coefficient versus Froude Number. At shallow depths and low speeds, a large lift is generated. The positive values of lift represent an upwards, "sea-suction" force on the body. It is this force which actual submarines must counter to remain submerged at periscope depth. Two local maxima and two local minima are observed. As with the drag coefficient, the maxima shift to the higher speeds at deeper depths. However, in contrast with the drag coefficient, the lift significantly decreases with increasing speed and becomes negative (downward force) at speeds above F = 0.55. For the shallowest depth, the second local maximum is almost four times smaller than the first local maximum. This correlates well to actual submarines, in which it is easier to remain submerged at higher speeds. Again, at the deepest depth, the oscillations appear as a straight line using the scale in Figure 10. Its lowest coefficient is 0.0462E-3 at the lowest speed, and it reaches a maximum of 0.126E-3 at F = 0.466 (a ratio of 2.74). So, the deepest depths do oscillate around a fairly constant

value, but the effect on the body is negligible compared with shallower depths. Thus, the shallowest depths and the lowest speeds exert the greatest lift force on the body.

The Moment Coefficient versus Froude Number, Figure 11, likewise displays an oscillatory characteristic. The negative values for the coefficient indicate that a bow-down moment is induced on the body, rotating the stern end towards the surface. This, too, agrees with the motion of actual submarines first broaching the surface at the stern. Two local maxima and two local minima are present as with the other two coefficients. Also, the shallowest depths produce the largest fluctuation in the coefficient. However, the magnitude of the coefficient greatly increases as the speed is increased. The oscillations appear less distinct as the depth increases, but the magnitude is clearly greater for higher speeds. The ratio of the local maxima for the shallowest depths is about three to one and drops to just over one for the deepest depths. As seen with the other two coefficients, the local maxima shift to the right (higher speeds) with increasing depth. In other words, at shallower depths the larger moment coefficient is produced at lower speeds. Also of note is the greater moment coefficient magnitude generated at lower speeds (below F = 0.35) as depth is increased above 0.15L. The moment coefficient causes the body to pitch down for all speeds and depths.

The wave making problem plots clearly display the results of summing the pressure distributions around the body. All three coefficients are oscillatory in nature. As the body is placed in deeper depths, the coefficients become smaller in magnitude. As speed is increased, drag and the bow-down moment increase, while lift decreases. The results correspond well to the operating experience of actual submarines at shallow depths.

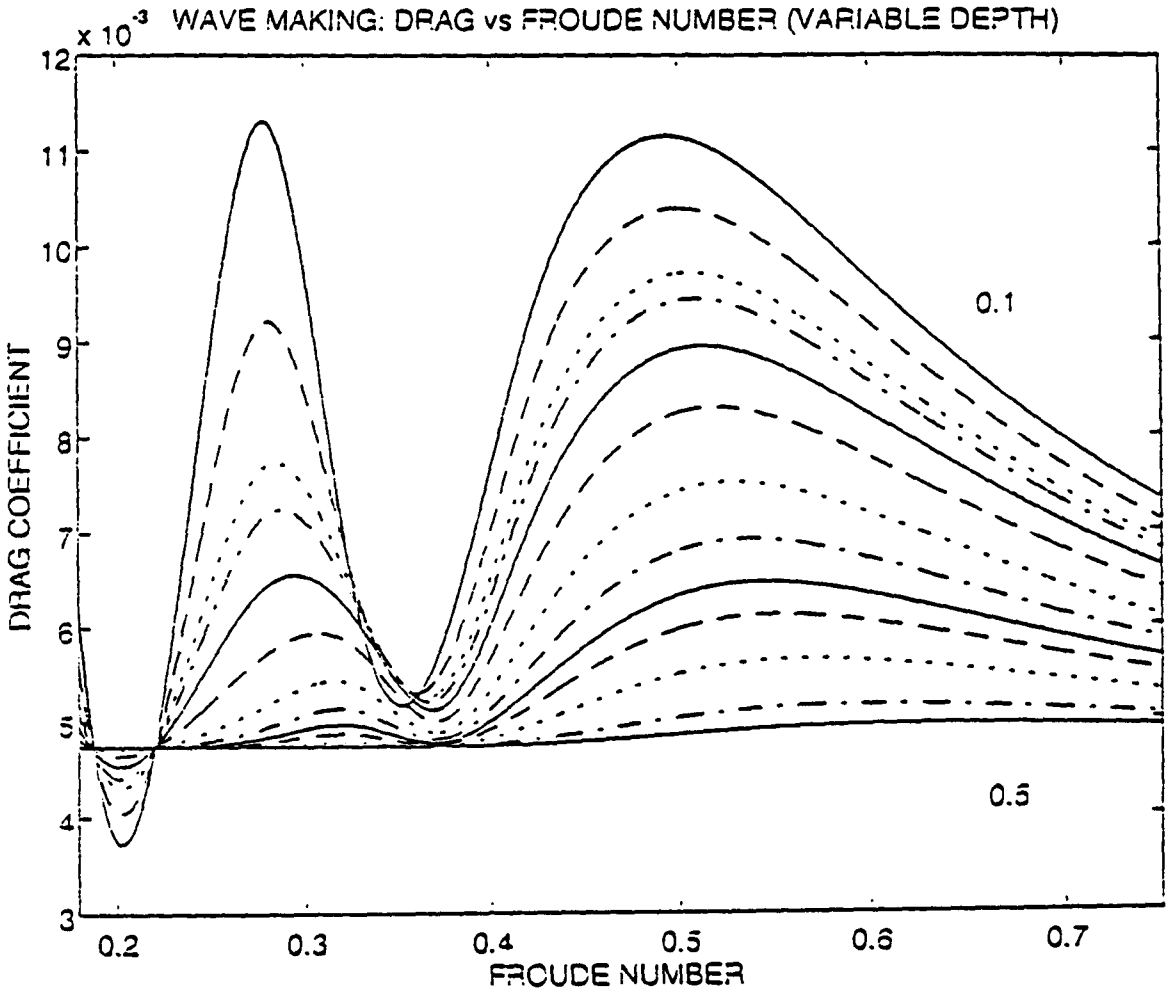

Figure 9: Wave Making: Drag Coefficient versus Froude Number

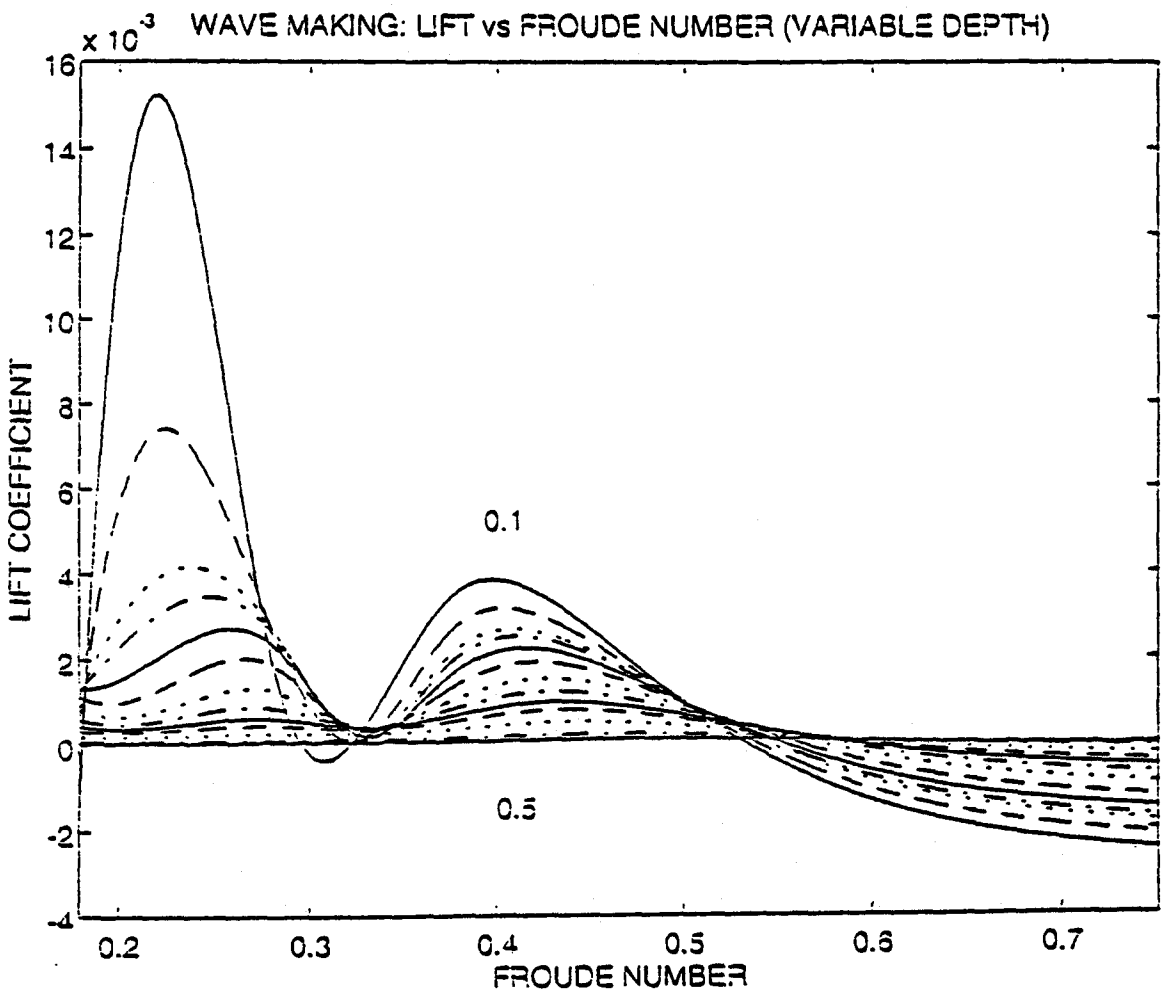

Figure 10: Wave Making: Lift Coefficient versus Froude Number

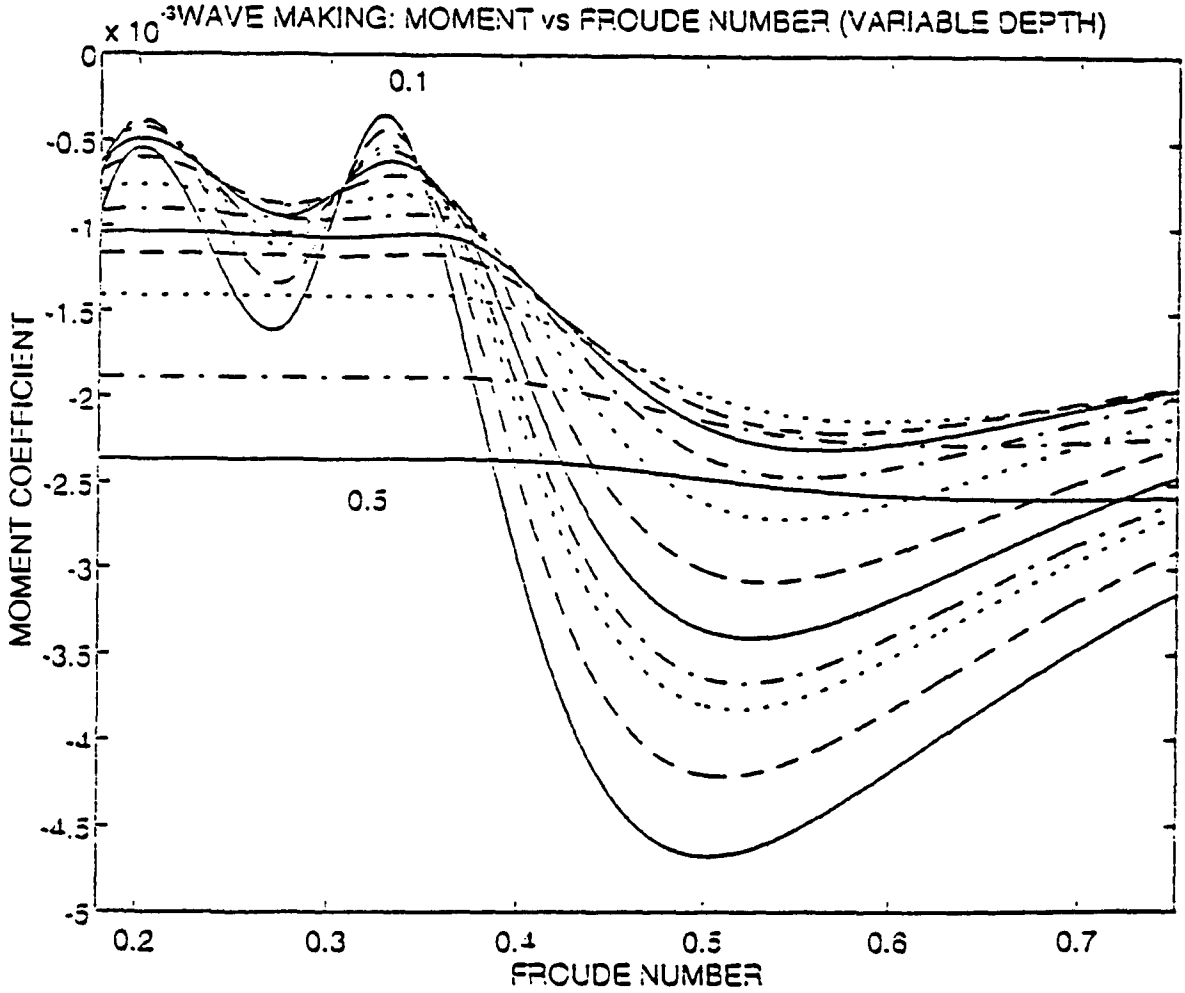

Figure 11: Wave Making: Moment Coefficient versus Froude Number

D. INCIDENT WAVES PROBLEM

After examining the body wave making problem, the effect of incident waves on the body is explored. The SUBOFF model was input to provide the program the body shape with which the incident waves interacted. Keeping only the second term of equation (65) and substituting the encounter frequency from equation (67) yielded the following pressure expression

$$p = -\frac{1}{2}\rho\omega_e^2 A^2 e^{2kz} \quad . \tag{76}$$

This pressure distribution was summed over all the panels to produce the drag, lift and moment coefficients. The drag and lift coefficient were normalized by $1/2\rho\omega^2A^2S$ and the moment coefficient was normalized by $1/2\rho\omega^2A^2SL$. For the various runs in this section, the depth, H, the body speed, U, the wave amplitude, A, the wave direction, θ, and the nondimensional wavelength, λ/L, were input to the program. Amplitude, A, was fixed at 1.0 and λ/L varied from 0.5 to 2.5 for all runs. The wavelength was directly obtained from the nondimensional wavelength and the wavenumber, $k = 2\pi/\lambda$, followed. The deep water wave frequency $\omega^2 = k/g$ was then obtained and used to calculate the encounter frequency, $\omega_e = \omega - (\omega^2/g)U\cos\theta$, where $\theta = 0°$ is following seas and $\theta = 180°$ is head seas. These parameters determined the pressure distribution through (75). All of the plots in this section

graph the coefficients versus the nondimensional wavelength, λ/L. Speeds are expressed as a Froude number, depth as a fraction of overall length and the wave direction, θ, as an angle in degrees. A positive lift coefficient represents an upwards (sea suction) force and a positive moment coefficient shows a bow-up moment. Three sets present the effects on the three coefficients. The first set examines the effect of depth as speed and wave direction are held constant. The next set varies the wave direction at a constant speed and depth, while the last set changes the body speed with depth and wave direction being fixed.

The first incident wave set looks at the exponential nature of the depth term for a given set of conditions. Hull speed was fixed at $F = 0.2$, and θ set at 90° (beam seas). This removed the effect of the body speed from the frequency of encounter. Depth was then varied between a tenth and a half of the overall body length. Figures 12 through 14 present the Drag, Lift and Moment Coefficients versus Nondimensional Wavelength, respectively. In each plot the coefficients rapidly decay as the depth is increased. The coefficients are negligible at a depth greater than 0.5λ ($0.5L$ times $1.0\lambda/L$). This validates the statement made in the problem formulation section that there is a negligible motion beneath a depth of 0.5λ. As the wavelength increases, the coefficients also increase at the deepest depths, showing that the longer waves have a larger effect on the body. However,

at the shallowest depth the coefficients decrease with increasing wavelength. Both the lift and moment coefficients peak at about 1.2λ/L then steadily drop as the waves lengthen. Overall, these plots clearly show the exponential decay of the coefficients with depth.

Figures 15 to 17 show the effects on the coefficients when the wave direction is varied. For these runs, depth was fixed at one tenth of overall length and body speed was set at F = 0.2. Wave direction was varied from 0° (following seas) to 180° (head seas) in 45° increments and are labelled as such. In each plot, the θ = 090 corresponds to the H = 0.1L curves of the variable depth plots. In the Drag Coefficient versus Nondimensional Wavelength plot (Figure 15), maximum drag is produced with head seas and steadily drops off as the seas move aft. The following seas are an order of magnitude smaller than the head seas. As the wavelength increases, the drag drops as the waves appear longer to the body. Figures 16 and 17, the Lift and Moment Coefficients versus Nondimensional Wavelength, show identical trends to one another. For head seas, both plots peak around a wavelength of one then steadily decrease as the wavelength increases. The head seas produce over twice the magnitude of the beam seas. This correlates well to at sea experience of being able to better maintain depth with beam seas than with head seas. For the following seas, the lift and moment coefficients both slowly increase

with wavelength, but lie significantly below the beam seas curve. Thus, head seas produce the largest coefficients and following seas yield the smallest coefficients.

Next, the effects on varying the body speed were examined. Figures 18 to 20 plot the Drag, Lift and Moment Coefficients versus Nondimensional Wavelength. In these runs, depth was fixed at one tenth of overall length and θ set to 180° (head seas). Speed was varied from F = 0.0 to 0.8 in 0.2 increments. The F = 0.2 curves correspond to the θ = 180 curves on the variable wave direction plots (Figures 15 to 17). Also, the F = 0.0 curves correspond to the H = 0.1L curves on the variable depth plots (Figures 12 to 14), since the effect of hull speed was taken out of these by using beam seas. Each plot clearly shows that the greater speeds produce the largest coefficients. From the lowest to the highest speeds, the coefficients change by an order of magnitude. Additionally, as the wavelength is raised, each of the coefficients slowly decays in magnitude. Thus, in examining the incident waves effects alone, a higher hull speed or a shorter wavelength would cause the most drag, the greatest lift and the largest bow-down moment.

The results of the incident wave runs clearly showed the effects on the SUBOFF model for various input conditions. The coefficients all dropped exponentially with depth as was predicted. Below 0.5λ, the incident waves are negligible. The head seas produced the greatest coefficients at all

wavelengths. Seas aft of the beam are significantly less important. The higher hull speeds yielded the largest coefficients at each wavelength. The lowest speed runs were equivalent to the beam seas plots.

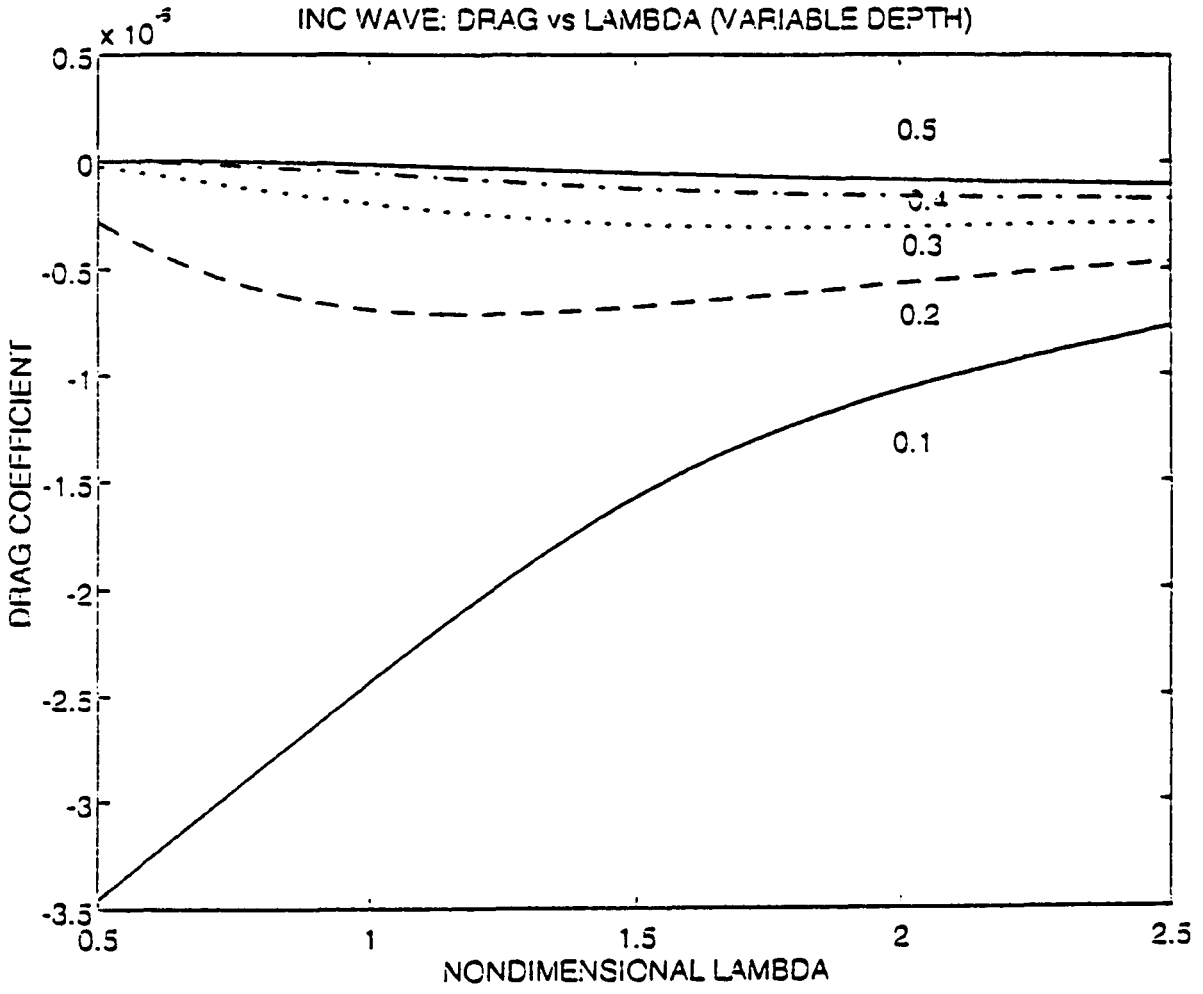

Figure 12: Incident Wave: Drag Coefficient versus Nondimensional Wavelength (Variable Depth)

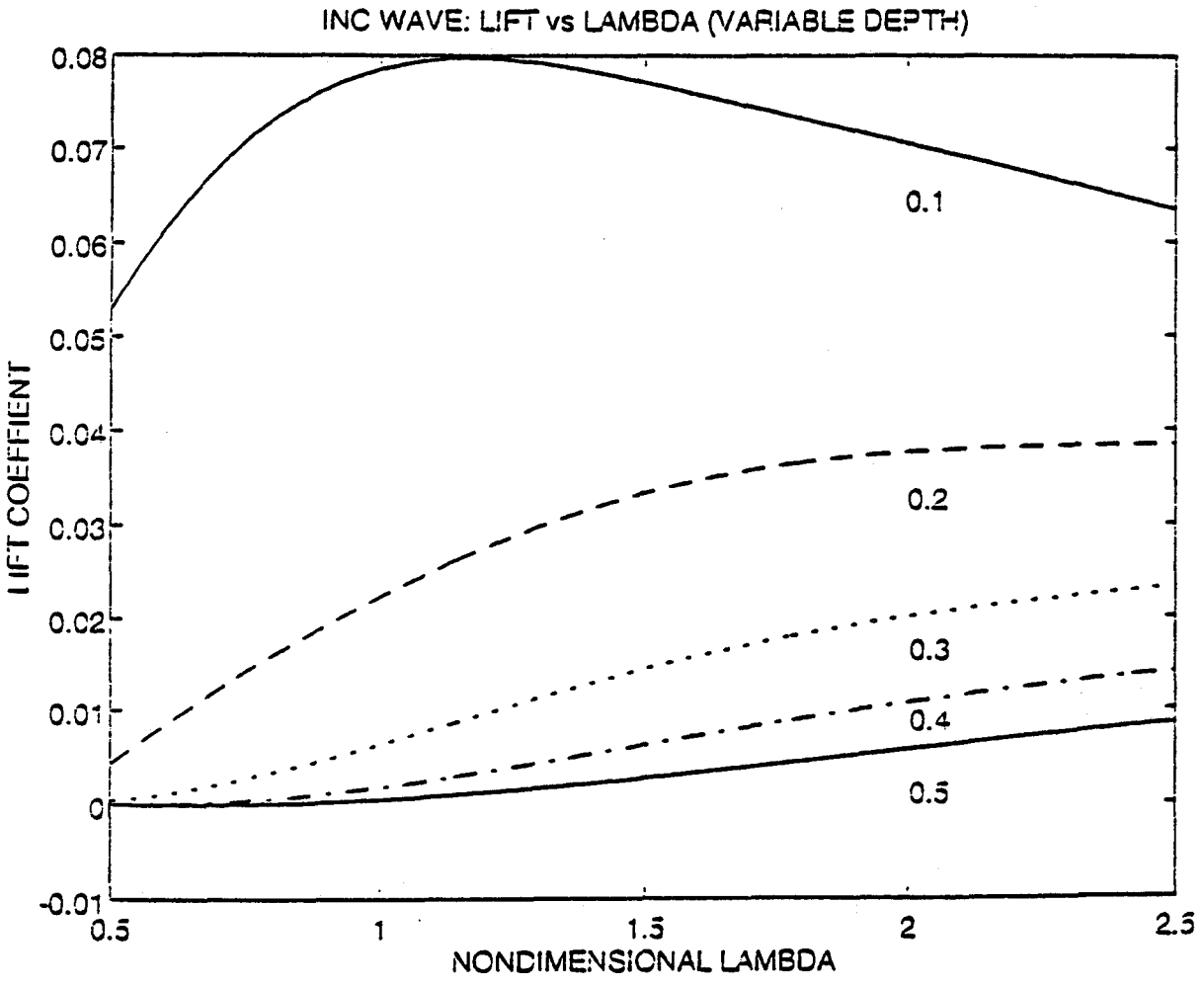

Figure 13: Incident Wave: Lift Coefficient versus Nondimensional Wavelength (Variable Depth)

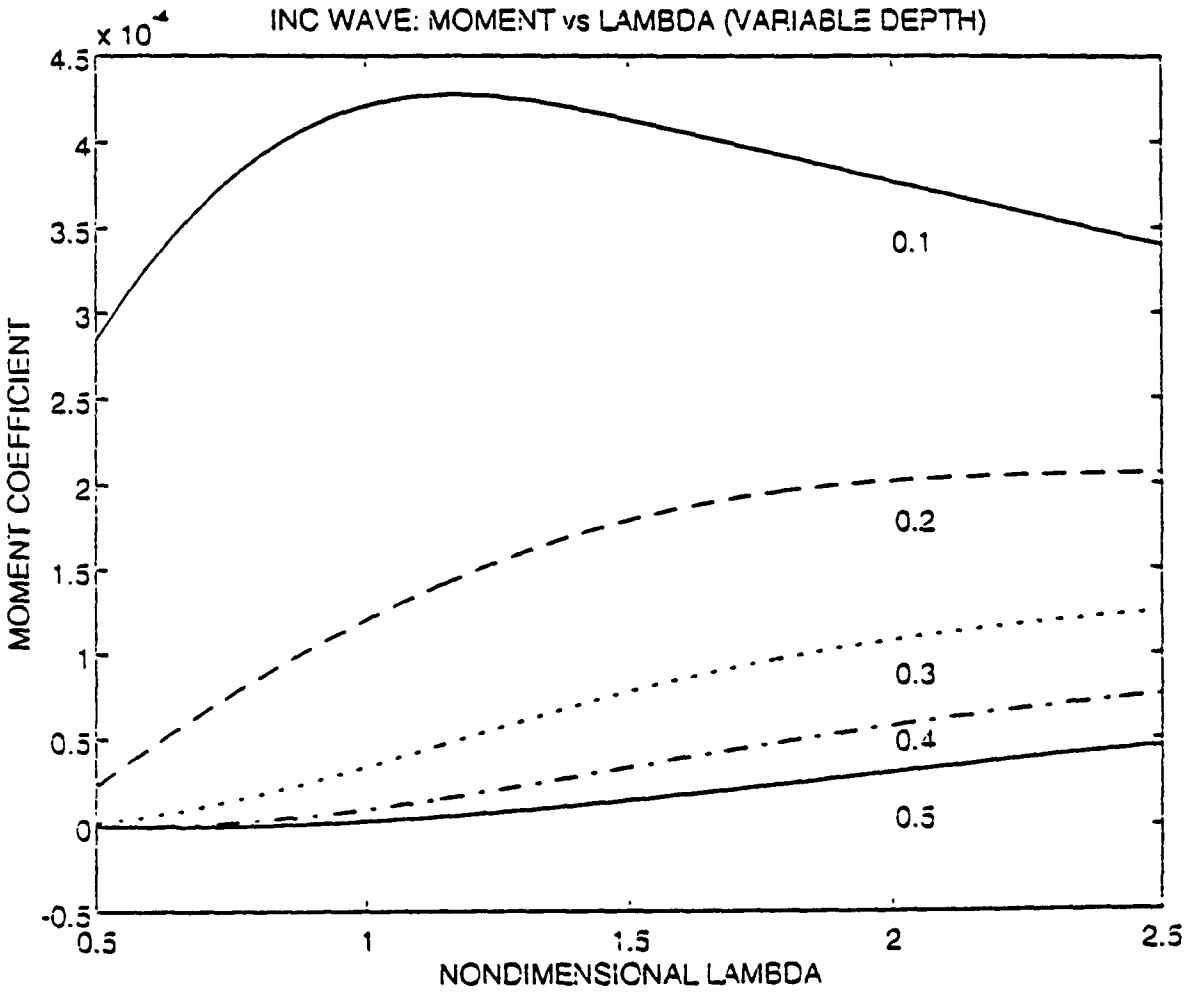

Figure 14: Incident Wave: Moment Coefficient versus Nondimensional Wavelength (Variable Depth)

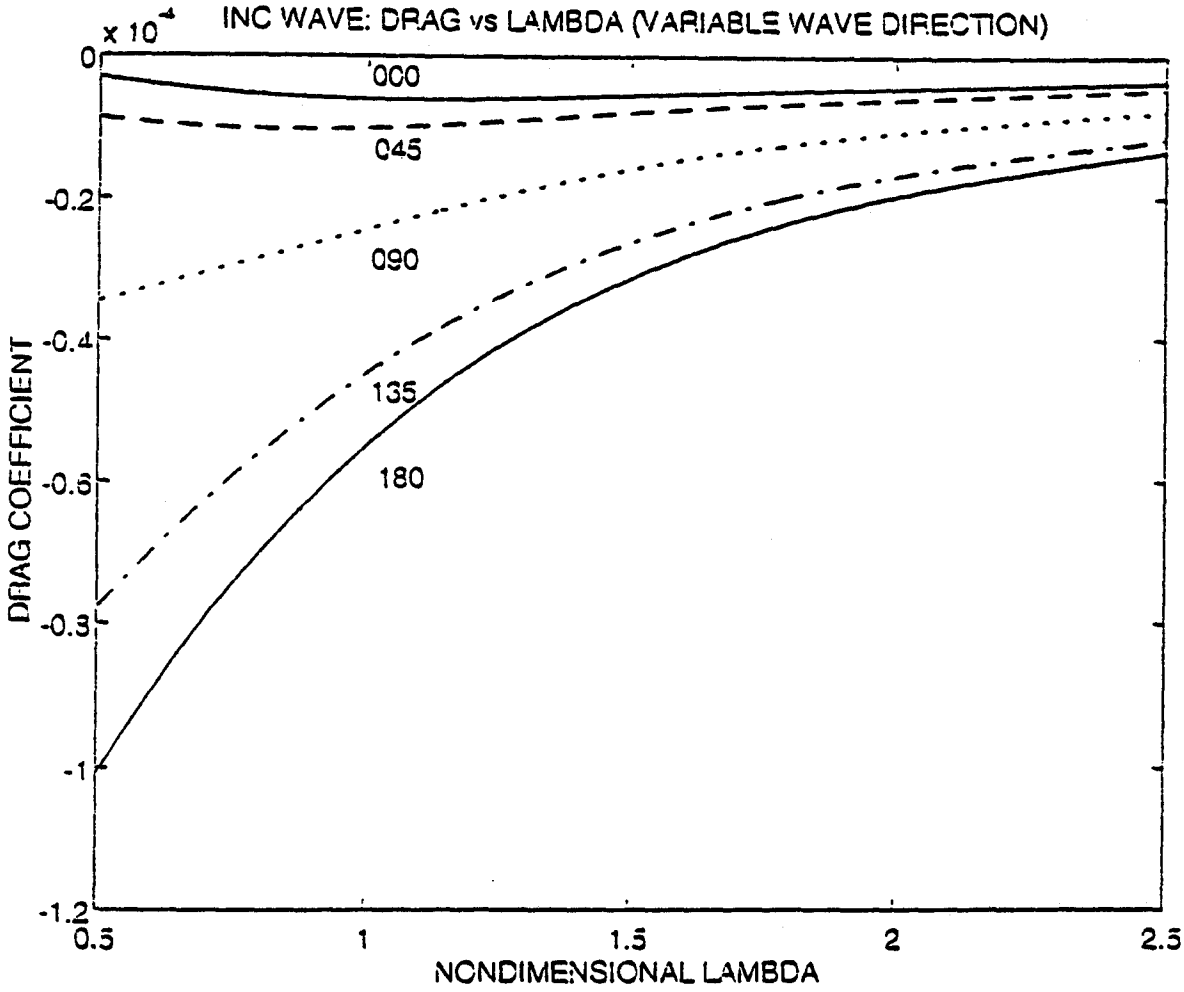

Figure 15: Incident Wave: Drag Coefficient versus Nondimensional Wavelength (Variable Wave Direction)

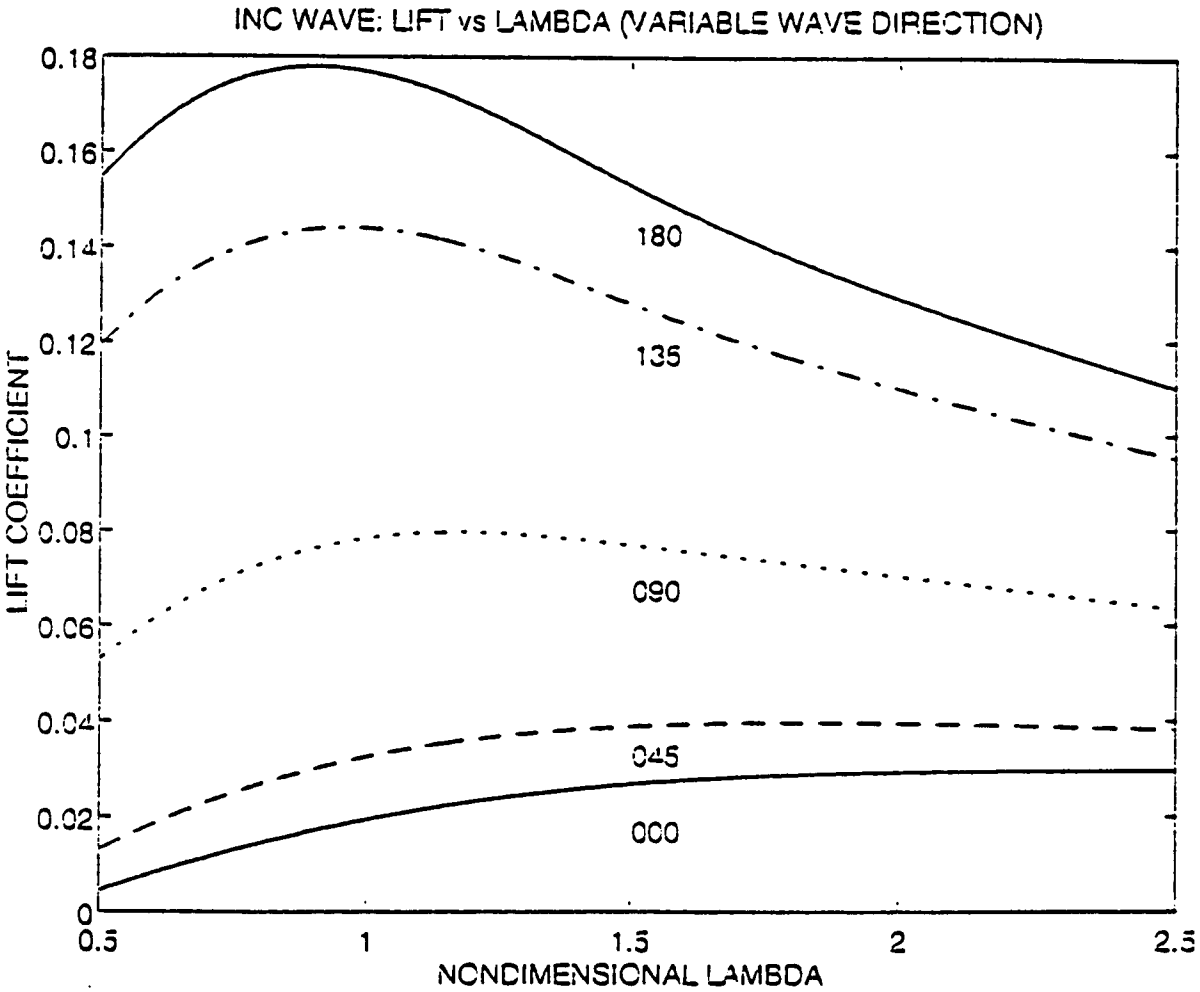

Figure 16: Incident Wave: Lift Coefficient versus Nondimensional Wavelength (Variable Wave Direction)

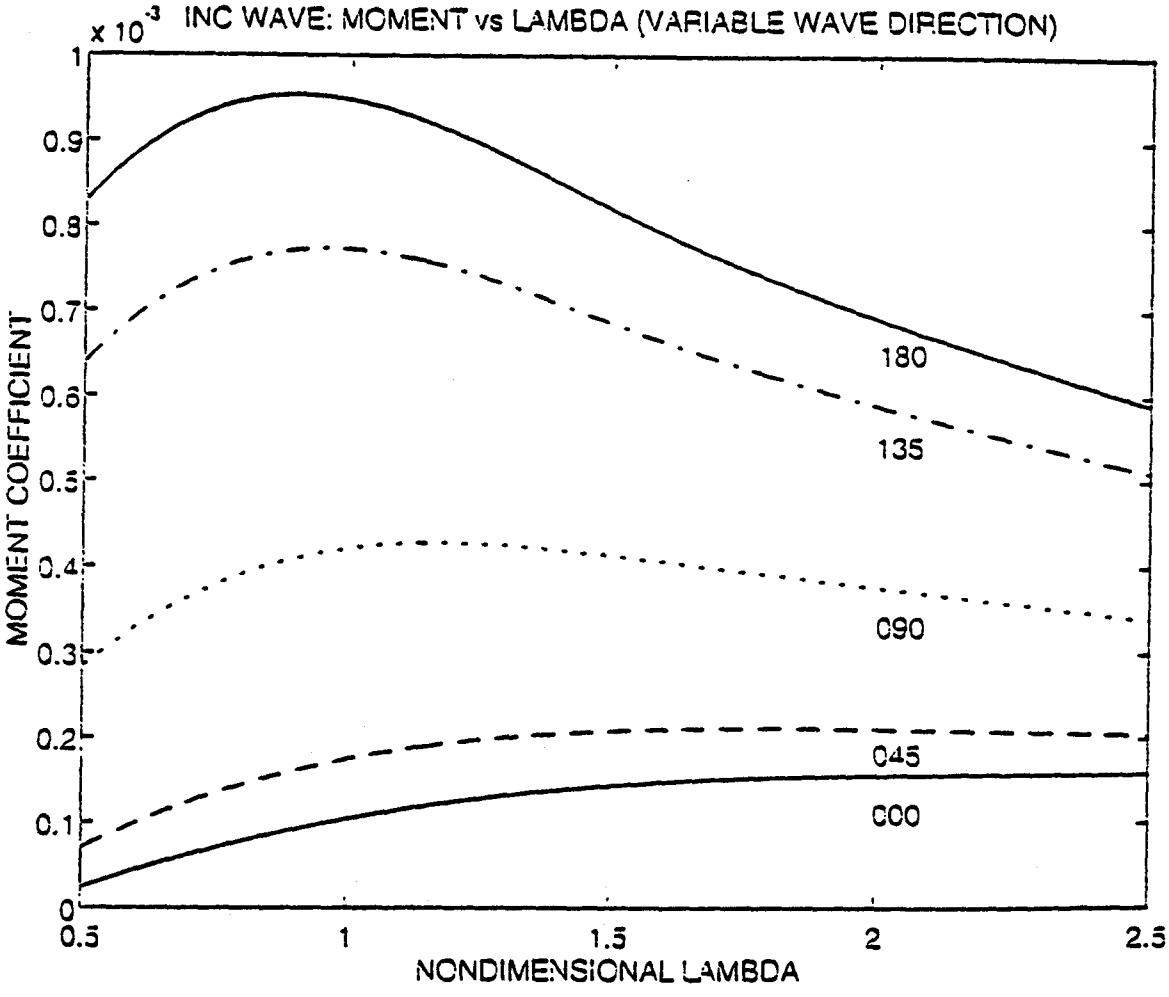

Figure 17: Incident Wave: Moment Coefficient versus Nondimensional Wavelength (Variable Wave Direction)

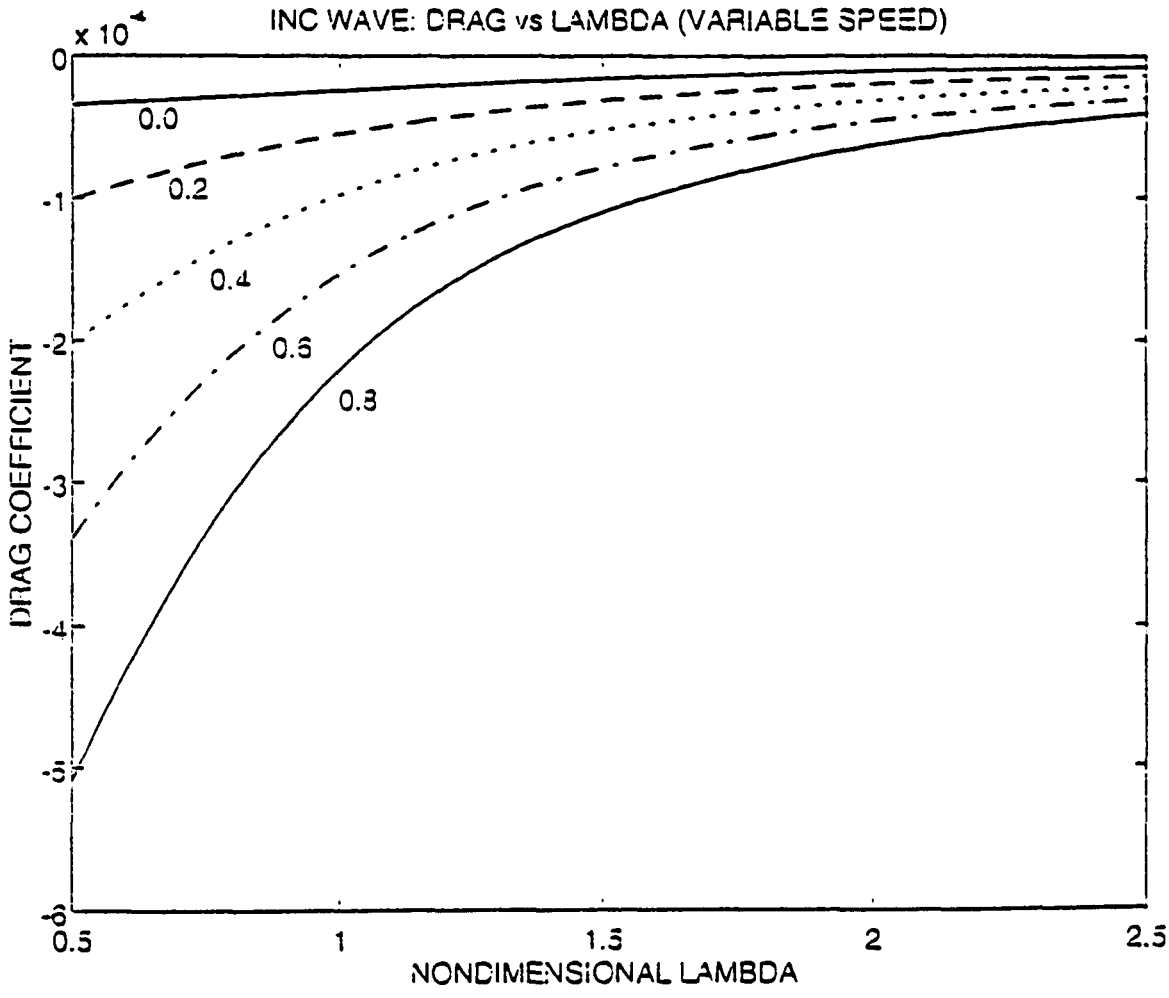

Figure 18: Incident Wave: Drag Coefficient versus Nondimensional Wavelength (Variable Speed)

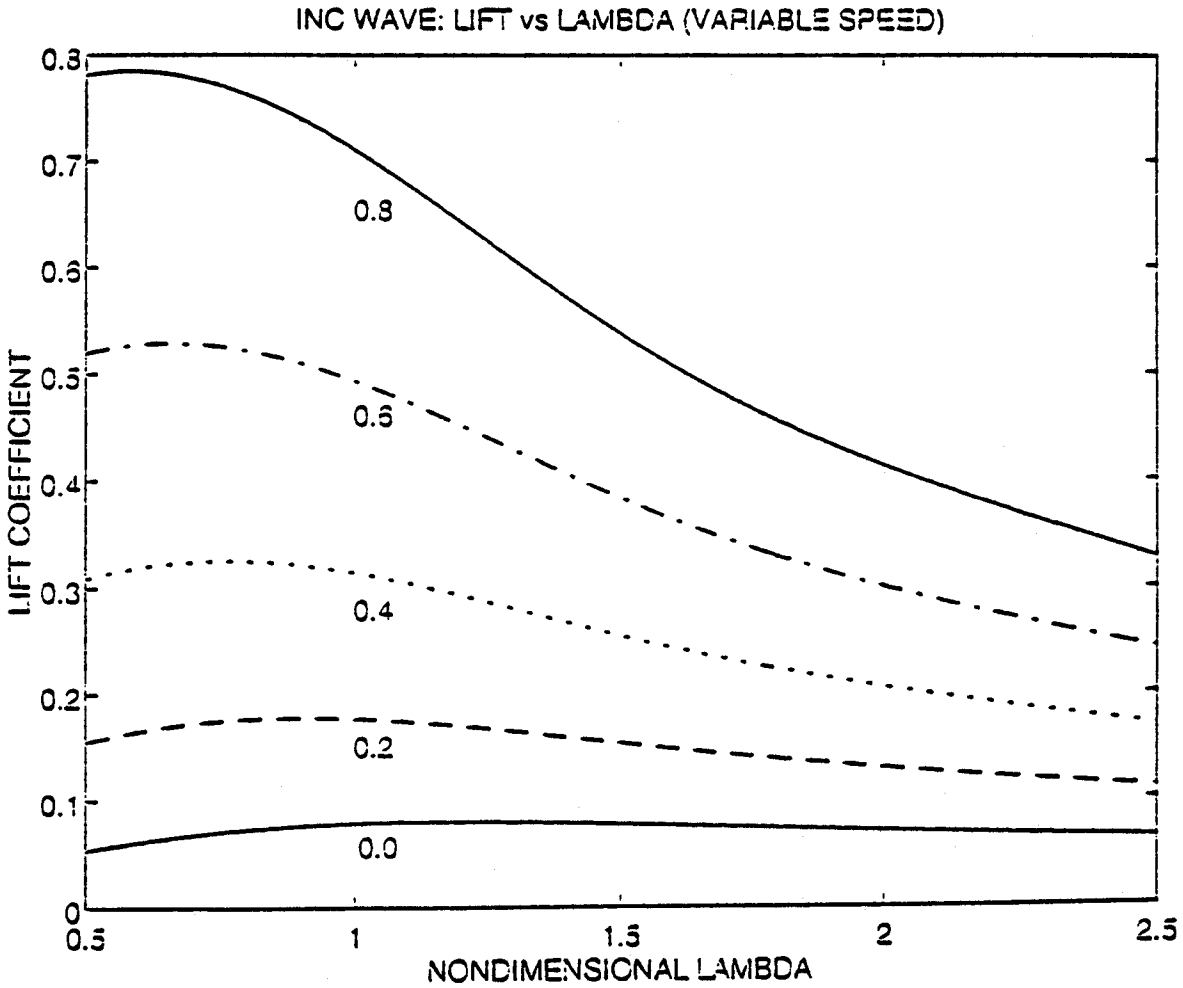

Figure 19: Incident Wave: Lift Coefficient versus Nondimensional Wavelength (Variable Speed)

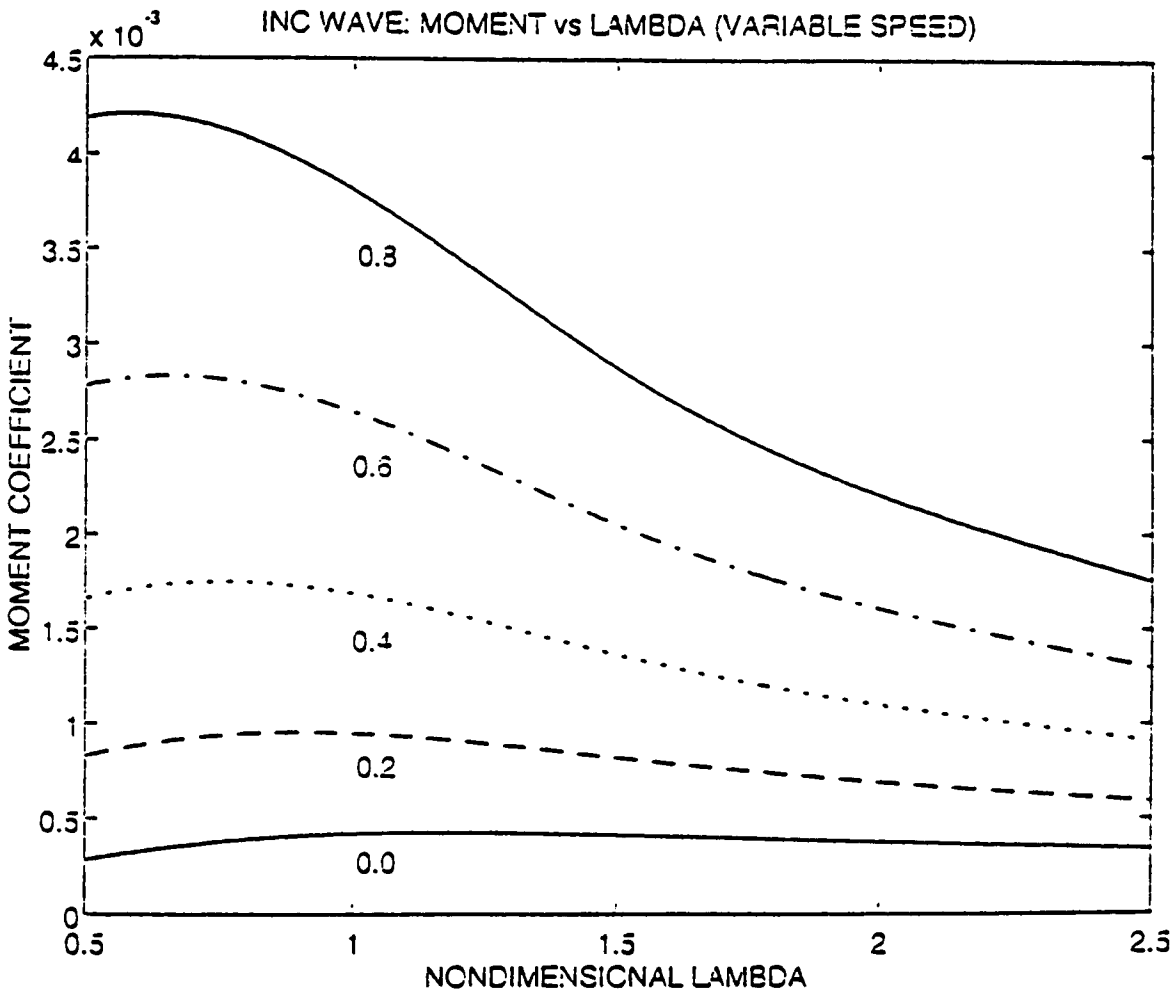

Figure 20: Incident Wave: Moment Coefficient versus Nondimensional Wavelength (Variable Speed)

E. SUMMARY

The results chapter constitutes the major part of this work. Using the DARPA SUBOFF model of a bare submarine hull, the hydrodynamic forces and moments produced from various sources was examined. A set of convergence runs established the number of vertical and θ-integration points at 8 and 16, respectively. These were utilized for the subsequent wave-making runs and the incident wave runs.

The wave-making runs produced oscillatory plots for each coefficient. The drag coefficient represented the longitudinal force opposing the hull's motion and this steadily declined with increasing depth. The lift coefficient showed the upwards, sea-suction force present on the body. At the shallowest depths and the slowest speeds, these sea-suction forces were the greatest. The moment coefficient explained how much the body would pitch up or down. As speed increased, the bow-down moment increased. Of these effects, the lift force has the greatest bearing on a submarine maintaining depth. Thus, using the greatest speed is the most advantageous to prevent broaching the submarine.

Finally, the incident wave runs showed the effects on the body from incident waves on an otherwise calm free surface. The incident waves are exponentially attenuated as depth is increased and at depths greater than half the wavelength, the effects are negligible. Head seas produce a larger lift and

moment than do beam or following seas, making it more difficult to maintain depth when driving a submarine into the seas. Upon examining the role of hull speed, it was found that the greatest speeds produced the most drag, the highest lift and the largest moment. Thus, the higher hull speed would increase the severity of the incident waves' lift.

Combining the wave making and incident wave results yields the total response on the hull. The total drag on the body reflects the resistance to the body's forward motion. The wave making runs produced positive (opposing) forces on the body while the incident wave runs yielded very small negative (aiding) forces on the body. The drags for each were calculated to make realistic comparisons. For the wave making runs the drag (D_{WM}) is

$$D_{IW} = C_D \frac{1}{2} \rho U^2 S \quad , \tag{77}$$

and for the incident waves the drag (D_{IW}) is

$$D_{IW} = C_D \frac{1}{2} \rho \omega^2 A^2 S \quad . \tag{78}$$

For the low speeds (F = 0.2) with head seas, D_{WM} = 0.765 lbf and D_{IW} = -0.00928 lbf. The two forces are of opposite signs, but the magnitude of the wave making drag greatly outweighs the incident wave drag. A similar effect is also seen at

higher speeds (F = 0.7) with D_{WM} = 1.61 lbf and D_{IW} = -0.0325 lbf. Thus, the majority of the drag on the submerged body is from wave making effects.

The total moment produced on the body directly affects the ability of the submarine to keep the stern (mainly) or bow from breaking the free surface. The wave making runs produced negative (bow-down) moments and the incident waves yielded positive (bow-up) moments. The moments for each run were calculated to make relevant comparisons. For the wave making runs the moment (M_{WM}) is

$$M_{WM} = C_M \frac{1}{2} \rho U^2 S L \quad , \tag{79}$$

and for the incident waves the moment (M_{IW}) is

$$M_{IW} = C_M \frac{1}{2} \rho \omega^2 A^2 S L \quad . \tag{80}$$

For the low speeds (F = 0.2) with head seas, M_{WM} = -1.44 ft-lbf and M_{IW} = 2.10 ft-lbf. This shows that the two moments are roughly equivalent and of opposite sign, thus cancelling out one another. As the seas move aft, M_{IW} drops to 0.93 ft-lbf off the beam and falls to 0.22 ft-lbf for following seas. For these cases, a total bow-down moment is produced, forcing the stern up to the surface. As speed is raised to F = 0.7, all the moments increase, except for the beam incident waves

which are independent of speed. M_{WM} rises dramatically to -123.4 ft-lbf while M_{IW} only increases to 7.30 ft-lbf for head seas and to 0.53 ft-lbf for following seas. Thus, a much greater bow-down moment is produced at higher speeds, resulting in more submarine control surfaces and variable ballast being needed to prevent the stern from breaking the free surface.

Even of greater importance to submarine depth control is the effect of the combined lift on the body. This is the primary item of interest since this upward force must be overcome to prevent the entire body from broaching the free surface. A combination of ship's speed, control surfaces and variable ballast are utilized to counter the lift force. In the wave making runs, higher ship speeds produced less lift, while greater speeds yielded more lift in the incident wave runs. To make the results meaningful, the lift forces in each case must be compared. For the wave making runs, the lift (L_{WM}) is

$$L_{WM} = C_L \frac{1}{2} \rho U^2 S \quad , \tag{81}$$

and for the incident wave runs the lift (L_{IW}) is

$$L_{IW} = C_L \frac{1}{2} \rho \omega^2 A^2 S \quad . \tag{82}$$

For the case of head seas with body speed being F = 0.2 and

nondimensional wavelength of one, L_{IW} = 27.84 lbf and L_{WM} = 3.02 lbf. When the seas come from the beam, L_{IW} = 12.37 lbf and when the seas are following, L_{IW} = 3.09 lbf. In all cases, both lifts are positive and the body is drawn to the surface. When speed is increased to F = 0.7 in head seas, L_{IW} significantly increases to 92.80 lbf, but L_{WM} changes sign and is of the same order of magnitude, -4.93 lbf. The upwards force from the incident head waves will greatly overcome the negative lift generated by the body. But, as the sea direction moves aft, the lift generated by the incident waves drastically drops. For beam seas, L_{IW} remains constant (independent of speed) and for following seas L_{IW} rises to 6.87 lbf. Thus, sea direction plays a major role in determining the lift which the submarine must counteract.

IV. PARAMETRIC STUDIES

A. INTRODUCTION

The previous chapter detailed the results of the wave making problem and the incident waves problem for a given body, namely the DARPA SUBOFF model. This chapter explores the effects of changing the body size and shape. The body is divided into three sections, with each section being defined by a set of coefficients. By varying the overall length in one case and by changing the maximum diameter in a second case, the effects on the drag, lift and moment coefficients are examined.

The body of revolution hull form was selected to model a submarine since it is described by simple geometric forms which are developed from elementary mathematical equations. Essentially, all cross sections of the hull are circular. The development of this approach is articulated in an article on submarine design concepts (Jackson, 1992). The hull form is composed of three sections. The forward end called the entrance, the parallel middle body and the after end called the run. The entrance is a portion of a parabola of revolution with length, L_f, of 2.4 diameters. The run is a portion of an ellipsoid of revolution with length, L_a, of 3.6

diameters. The parallel middle body is a cylinder of maximum diameter, D, with length, L_{PMB}.The sum of L_a, L_f and L_{PMB} is the overall length, L.

If one were to use equations for true ellipsoids and parabolas, the entrance and run would be too fine for a modern submarine hull form. The body size is increased by using large exponents (n_f and n_a) in the equations below.

$$y_f = \frac{D}{2}\left[1 - \left(\frac{x_f}{L_f}\right)^{n_f}\right]^{\frac{1}{n_f}} \tag{83}$$

$$y_a = \frac{D}{2}\left[1 - \left(\frac{x_a}{L_a}\right)^{n_a}\right] \tag{84}$$

Figure 21 is a drawing of the hull shape which details the various lengths. Here x_f and x_a are the offsets from the maximum diameter, and y_f and y_a are the hull radii at their respective offsets.

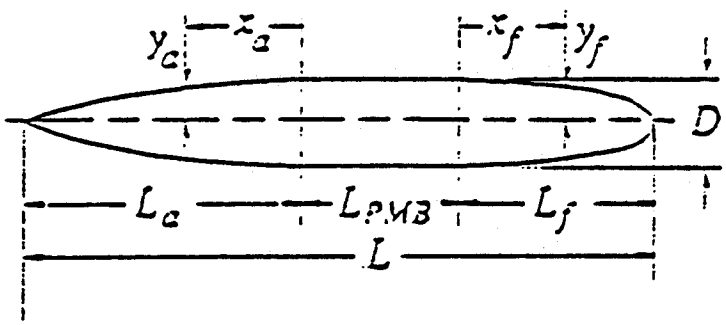

Figure 21: Submarine Hull Shape

Using these parameters, the total volume of the body can be calculated as the sum of the volumes of the entrance, V_f, the run, V_a, and the parallel middle body, V_{PMB}:

$$V_f = \pi \left(\frac{D}{2}\right)^2 [C_{pf} * 2.4 * D] \tag{85}$$

$$V_a = \pi \left(\frac{D}{2}\right)^2 [C_{pa} * 3.6 * D] \tag{86}$$

$$V_{PMB} = \pi \left(\frac{D}{2}\right)^2 [L - 6 * D] \tag{87}$$

where C_{pf} and C_{pa} are the prismatic coefficients for the entrance and run, respectively. Substituting y_f and y_a for D/2 and integrating over the length of each section yields

$$C_{pf} = \int_0^1 (1 - (x)^{n_f})^{\frac{2}{n_f}} \, dx \tag{88}$$

$$C_{pa} = \int_0^1 (1 - (x_1)^{n_a})^2 \, dx_1 \tag{89}$$

where $x = x_f/L_f$ and $x_1 = x_a/L_a$. Adding the three volumes and rearranging results in

$$V = \frac{\pi D^3}{4}\left[3.6C_{pa} + \frac{L_{PMB}}{D} + 2.4C_{pf}\right] \quad . \qquad (90)$$

In performing the parametric studies, the volume (displacement) was kept constant and set equal to the SUBOFF's displacement. The SUBOFF model was slightly different than the bodies of revolution described above, in that the entrance was twice the diameter and the run was 2.18 times the diameter. Yet, the shape of each SUBOFF section was certainly circular. In the first study, the displacement and the diameter of the body were fixed and the length was varied through the use of different exponents for the entrance and the run. In the second study, the displacement and the overall length were fixed and the diameter changed with various exponents. In both studies, wave making and incident wave runs were conducted.

B. EFFECTS OF LENGTH

The first parametric study examined the effects on the drag, lift and bow-up moment coefficients as the overall length was varied. The displacement was fixed at 24.692 ft^3 and the maximum diameter held at 1.667 ft. All parameters remained the same, except that overall length varied in each run and depth was set at one tenth of the length. For each

run, equal values of the exponents n_a and n_f were chosen. From these exponents, the prismatic coefficients were obtained from (88) and (89). Then, from (90), the length of the parallel middle body, L_{PMB}, was found which set the overall length, L. Table II summarizes the exponents, prismatic coefficients and overall lengths utilized in this parametric study. As the exponent increased in value, the entrance and the run became wider and rounder; i.e., more cylindrical throughout. Also, the overall body length became shorter. The longitudinal stations and their respective radii were calculated and converted into the correct input format. The y and z values were calculated as in previous runs. As before, the computer program output the three coefficients which are shown in Figures 22 to 33. The graphs plot the drag, lift, and moment coefficients versus speed (Froude number) for the wave making runs and plot the coefficients versus nondimensional wavelength for the incident wave runs. In each plot, the $n_a = n_f = 2.0$ and the $n_a = n_f = 4.0$ curves are labelled, with the other four curves lying sequentially between these two labelled curves. Each plot will be separately detailed.

TABLE II. PRISMATIC COEFFICIENTS AND OVERALL LENGTH

$n_a=n_f$	C_{pa}	C_{pf}	L
2.0	0.5333	0.6667	15.5
2.5	0.5952	0.7500	14.7
3.0	0.6429	0.8061	14.2
3.5	0.6806	0.8455	13.9
4.0	0.7111	0.8740	13.6
4.5	0.7366	0.8944	13.3

Figures 22 to 24 detail the wave making runs. The Wave Making Drag Coefficient versus Froude Number plot (Figure 22), shows an oscillatory character. As the exponents are raised, the curves show larger fluctuations in amplitude. Additionally, the local minima and maxima shift to the right as the exponents increase. The general shape of each curve is identical, with each curve slowly decreasing in magnitude above about F = 0.5. Overall, the magnitude increases by a factor of 4 from $n_a = n_f = 2.0$ to $n_a = n_f = 4.5$. The relative order of magnitude and the general sinusoidal shape is similar to the drag coefficient for the SUBOFF model. Thus, as the body becomes shorter and rounder, the drag force increases.

The Wave Making Lift Coefficient versus Froude Number plot (Figure 23) also shows an oscillatory character. Two local maxima are evident, with the second peak being of greater magnitude than the first. As the exponents are raised, the lift coefficient is increased. Also, the speed at the peak is shifted slightly to the right. Of special note is the decrease in magnitude above F = 0.43, with a change in sign above F = 0.56. As seen in the SUBOFF model, increasing speed above this point results in a downward, vice an upward, sea-suction force. Overall, the shorter, rounder hulls experience a greater lift force (almost double) than do the longer, thinner hulls.

Likewise, the Wave Making Moment Coefficient versus Froude Number plot (Figure 24) is oscillatory in nature. With the exception of a few low speed points, all values are negative, indicating a bow-down or stern-up moment. The magnitude of the coefficient increases as speed is raised to about F = 0.5 indicating that a higher moment is produced at higher speeds. But above F = 0.5, the magnitude slowly drops. The shorter, rounder hulls produce a greater bow-down moment than do the longer, thinner hulls. Thus, it is easier to keep the stern submerged with a longer, thinner model.

Figures 25 to 27 detail the incident wave runs. The Incident Wave Drag Coefficient versus Nondimensional Wavelength plot (Figure 25) shows that the magnitude decreases as the wavelength increases. Doubling the wavelength drops

the drag coefficient by a factor of two. Thus, as the waves become longer, the drag on the body is reduced. For the two lowest exponents, the drag is a positive value (opposing force) while the larger exponents are negative (aiding force). The more streamlined bodies (lower exponents) will experience resistance to their motion while the shorter, rounder bodies will actually be pushed in the longitudinal direction.

Figure 26 details the Incident Wave Lift Coefficient versus Nondimensional Wavelength plot. The lift coefficient is positive throughout (sea-suction force), peaks at a wavelength of about one, then linearly decreases. As the exponent is increased, the lift coefficient rises through all wavelengths. However, the change is relatively small as the lift coefficient varies only about 25 percent from the lowest to highest exponent. Thus, the shorter, rounder bodies experience a somewhat greater lift force.

Finally, the Incident Wave Moment Coefficient versus Nondimensional Wavelength plot (Figure 27) displays a similar shape to the lift coefficient plot. The moment coefficients are positive, indicating a bow-up moment. As the exponent is raised, the moment coefficient is increased. About a 20 percent increase is noted from the lowest to the highest exponent. The four highest coefficients form a common curve above a wavelength of 1.5. Thus, the shorter, rounder body will feel a greater bow-up moment.

Varying the length while maintaining the displacement and maximum diameter constant result in changes to each of the three coefficients. Combining the effects of the wave making and incident wave runs, the following observations are made for the shorter, rounder bodies (higher exponents). They produce greater drag, which is due mainly to the wave making effects. The incident waves make these bodies more susceptible to sea-suction forces. Also, the largest bow-down moments are presented to these bodies. The second parametric study examines the role of a varying diameter.

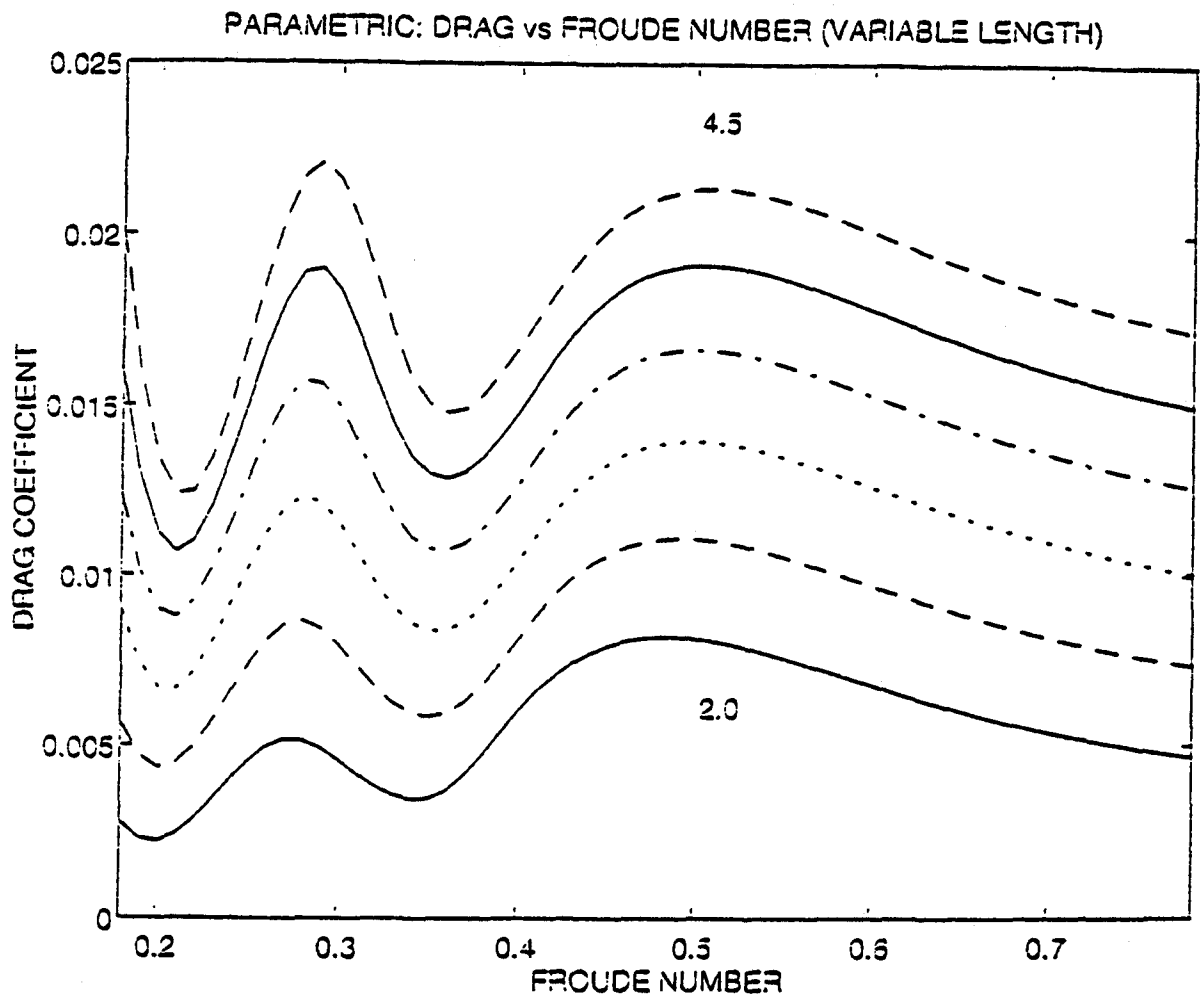

Figure 22: Parametric Study of Wave Making: Drag Coefficient versus Froude Number (Variable Length)

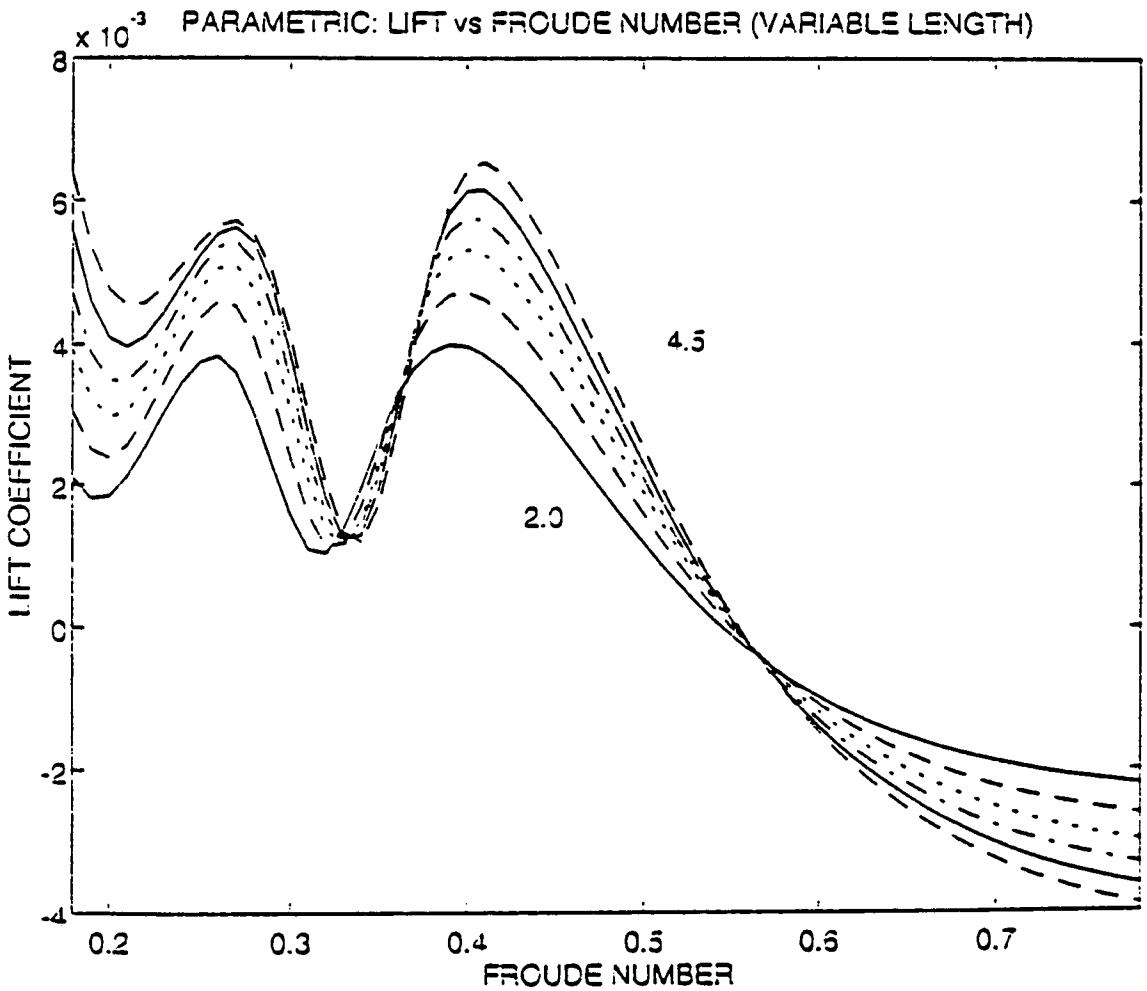

Figure 23: Parametric Study of Wave Making: Lift Coefficient versus Froude Number (Variable Length)

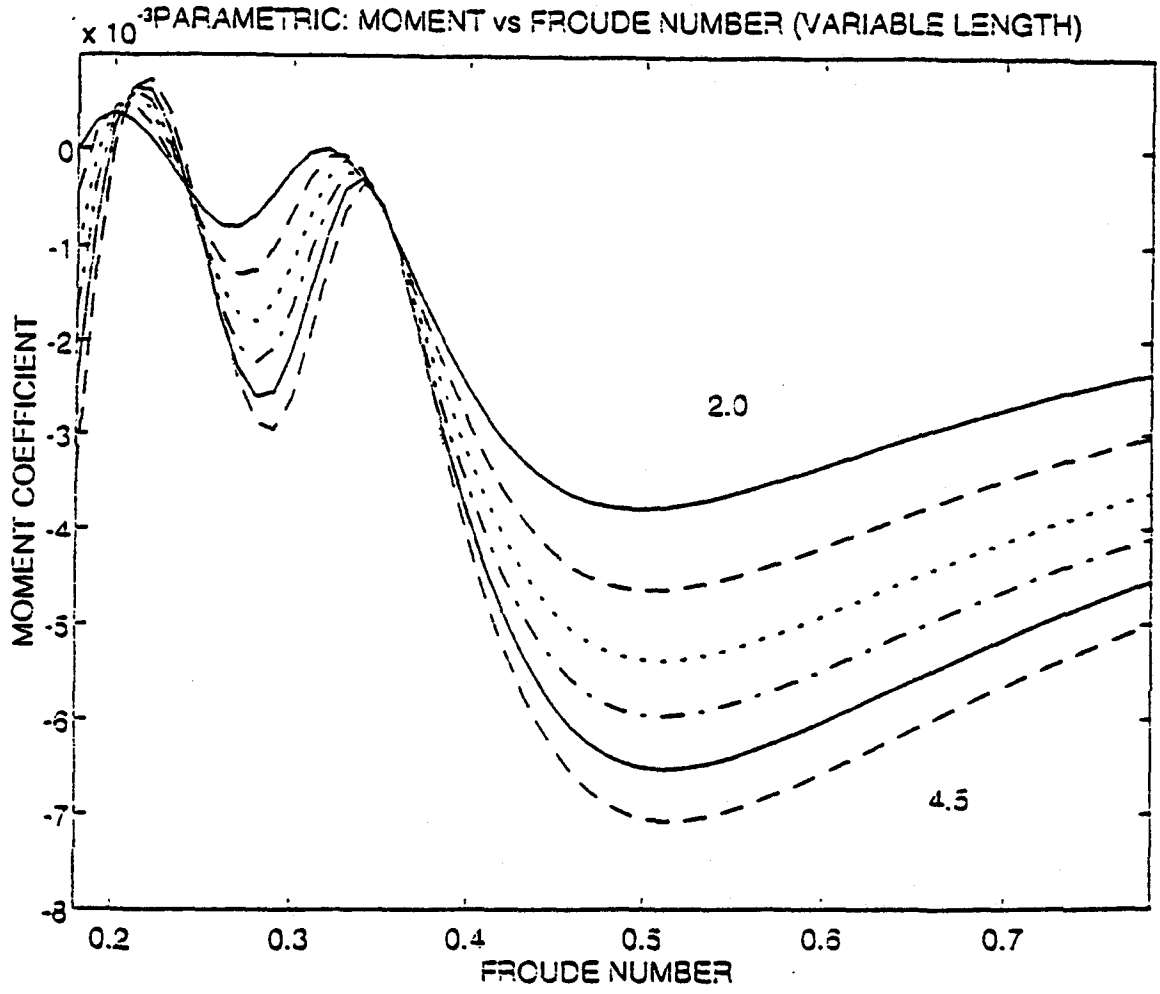

Figure 24: Parametric Study of Wave Making: Moment Coefficient versus Froude Number (Variable Length)

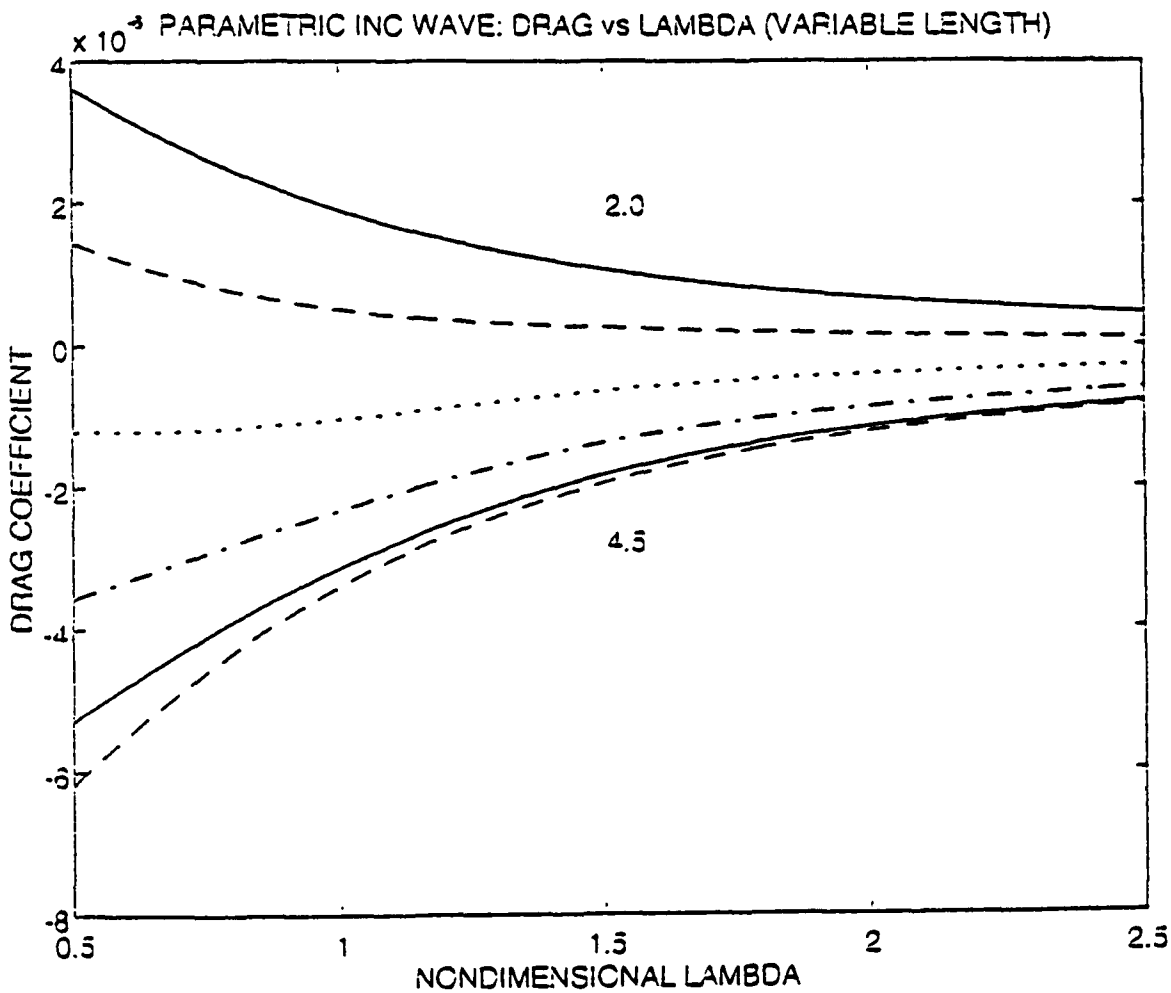

Figure 25: Parametric Study of Incident Waves: Drag Coefficient versus Nondimensional Wavelength (Variable Length)

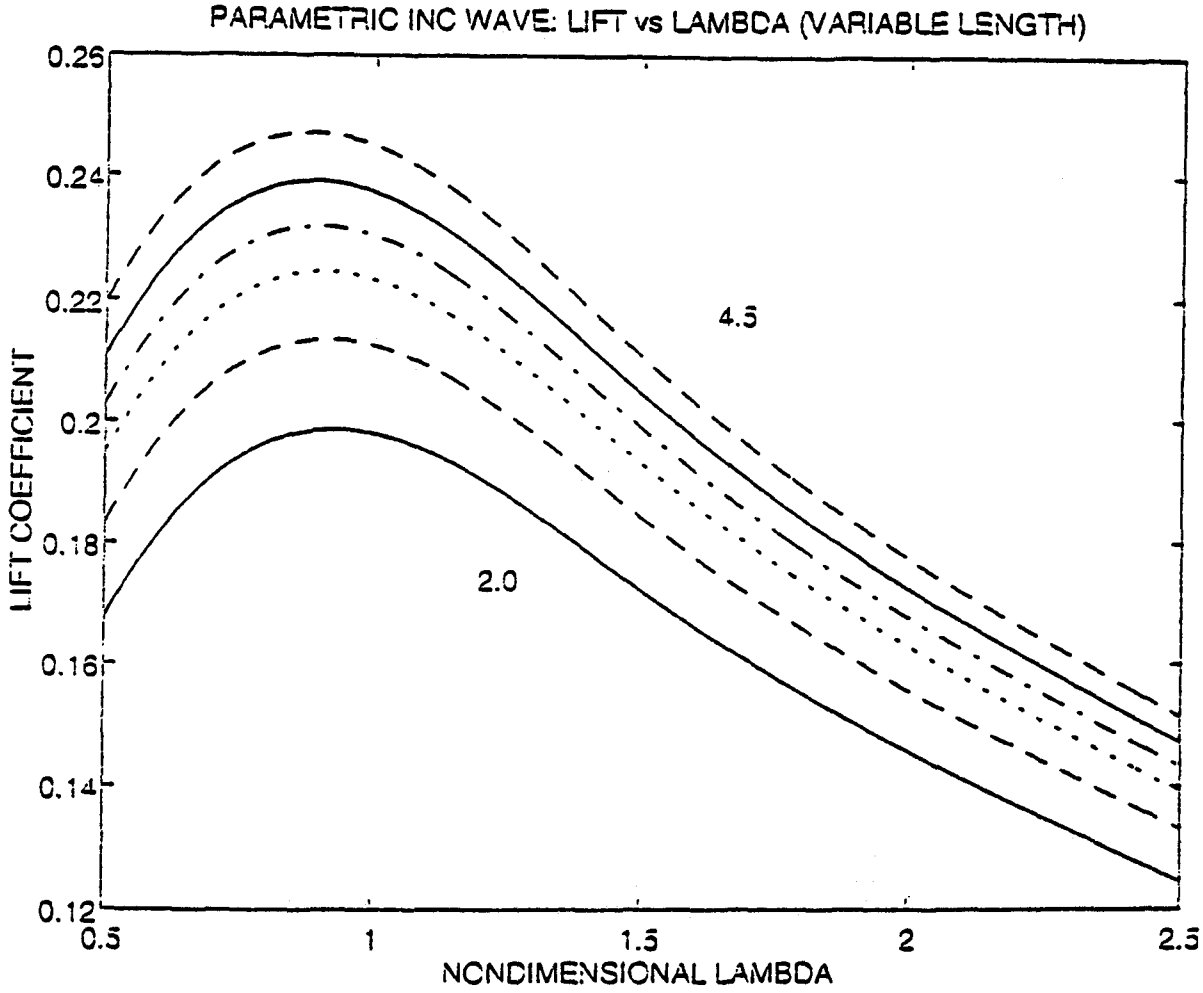

Figure 26: Parametric Study of Incident Waves: Lift Coefficient versus Nondimensional Wavelength (Variable Length)

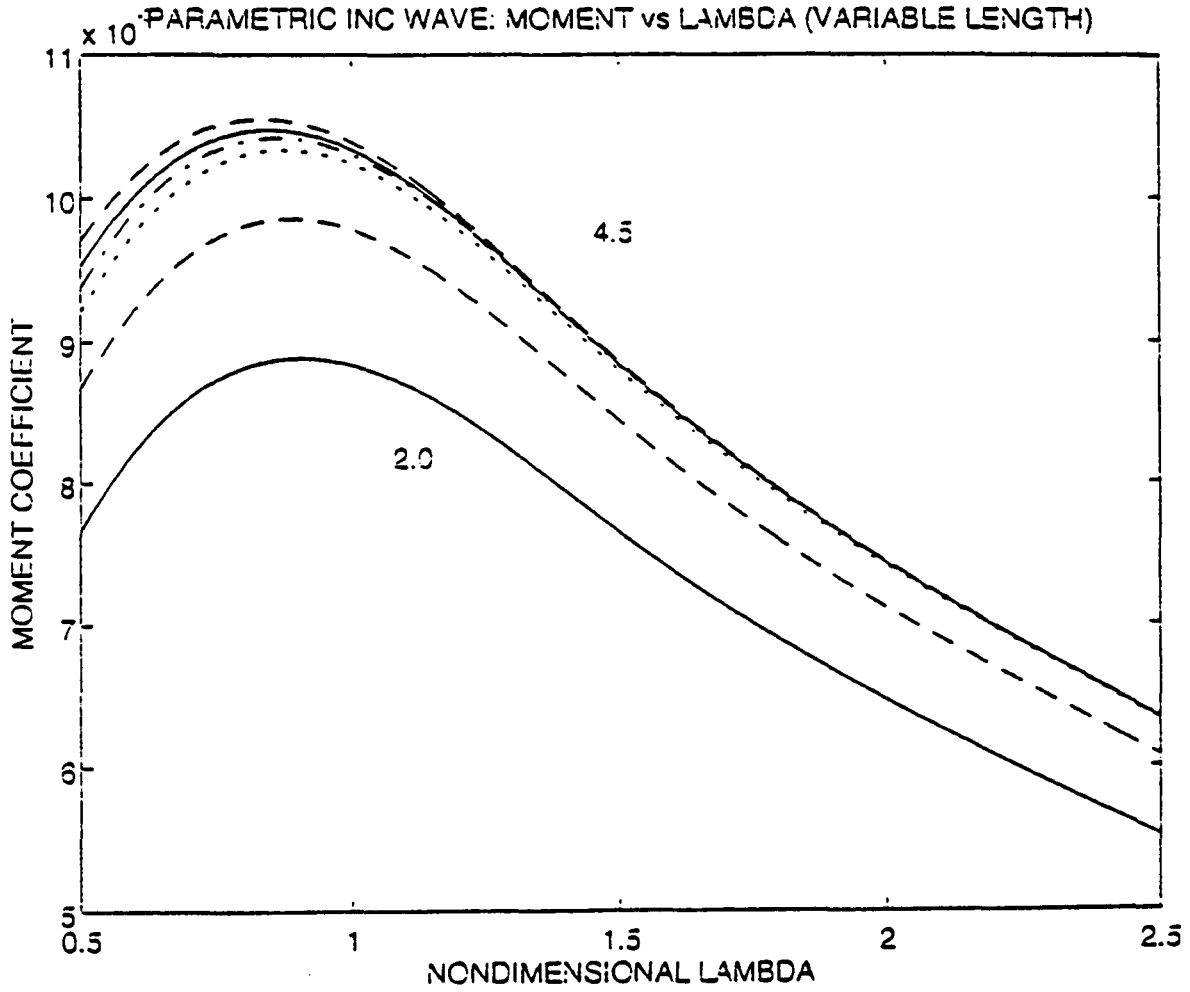

Figure 27: Parametric Study of Incident Waves: Moment Coefficient versus Nondimensional Wavelength (Variable Length)

C. EFFECTS OF DIAMETER

In the second parametric study, the displacement again remains constant at 24.692 ft^3, and the overall length and depth are fixed at 14.3 ft and 1.43 ft, respectively. In each run, the diameter is the variable and the effects on the drag, lift and bow-up moments are examined. The diameter for each is obtained by finding the roots of (90) for D. Again the values of exponents determine the prismatic coefficients (see Table II). The root closest to 1.667 (the original diameter) is chosen for the body diameter. Table III presents the exponents and their corresponding diameters.

TABLE III. EXPONENTS AND CORRESPONDING DIAMETERS

$n_a = n_f$	DIAMETER (ft)
2.0	1.78
2.5	1.71
3.0	1.66
3.5	1.63
4.0	1.61
4.5	1.59

As the Table III clearly shows, the larger exponents result in smaller diameters to maintain the same displacement. As the ends become more rounded, the maximum diameter must be reduced. The results generated by the computer program are shown in Figures 28 to 30 for the wave making runs and in Figures 31 to 33 for the incident wave runs.

An oscillatory set of curves is obtained for the Wave Making Drag Coefficient versus Froude Number plot (Figure 28). Two peaks are observed, with the peaks shifting to higher speeds as the exponents increase. As the exponents are raised, the magnitude of the drag coefficient increases, and is more than doubled from the lowest to the highest exponent. As the body becomes rounder on the ends and thinner in the middle, the drag force produced on the body increases.

Figure 29 details the Wave Making Lift Coefficient versus Froude Number for each exponent. The oscillatory nature is again apparent, but the shapes of each curve shows larger variations at lower speeds. For increasing exponents the first peak shifts slightly to the right and the magnitude increases while the second peak shifts to higher speeds and the magnitude decreases. As in the varying length study, above F = 0.55, all lift coefficients drop below zero. At lower speeds, the body produces an upward force and at higher speeds a downward force is produced. The rounder, thinner (greater exponents) body produces the greatest lift only in a

small region about F = 0.3. In the other lower speed regions (less than F = 0.55), the less rounded, fatter (lower exponents) body produces the higher sea-suction force. Thus, to reduce the effects of sea-suction forces, a rounder, thinner body would be preferable. Once again, higher speeds mitigate the sea-suction forces.

The last plot (Figure 30) shows the Wave Making Moment Coefficient versus Froude Number for various exponents. Once again, the oscillatory nature and the negative (bow-down) moment coefficients are present. A tighter set of curves is obtained than for the variable length case. At lower speeds (less than F = 0.35), the higher exponents yield the greatest coefficient magnitudes, while the higher speeds (F = 0.35 to F = 0.6) result in lower coefficient magnitudes. The less rounded, fatter bodies result in almost no moment at low speeds, but produce a larger moment as speed was increased. The rounded, thinner bodies produce a more uniform moment throughout the range of speeds encountered. Overall, every body form experiences a bow-down moment.

Figures 31 to 33 detail the incident wave runs as the diameter is varied. The Incident Wave Drag Coefficient versus Nondimensional Wavelength plot (Figure 31) shows a decreasing magnitude coefficient throughout all wavelengths. Similar to the varying length case, the the lowest exponents yield positive coefficients, while the highest exponents produce negative drag coefficients. As the body becomes rounded and

narrow (higher exponent), the incident waves actually aid the body's motion instead of opposing it. Still, the effects are very small when compared to the wave making case.

Figure 32 details the Incident Wave Lift Coefficient versus Nondimensional Wavelength plot. A peak near a wavelength of one is seen with a steady decline thereafter. As the exponents increase, theposition lift decreases slightly (about five percent). This shows that a thinner, rounder body will experience a smaller sea-suction force than a wider, streamlined body.

The last plot, Figure 33, displays the Incident Wave Moment Coefficient versus Nondimensional Wavelength. A similar shape to the varying length plot is observed. As the exponents increase from lowest to highest, the positive (bow-up) moment decreases by about 40 percent. As with the lift coefficient, the thinner, rounder body will feel a smaller bow-up moment than a wider, streamlined body.

In summary, changing the maximum diameter and the body shape for a given length and displacement modify each of the three coefficients. The less wider, streamlined (lower exponent) body produces the lowest drag, the greatest sea-suction force, and the most variable bow-down moment.

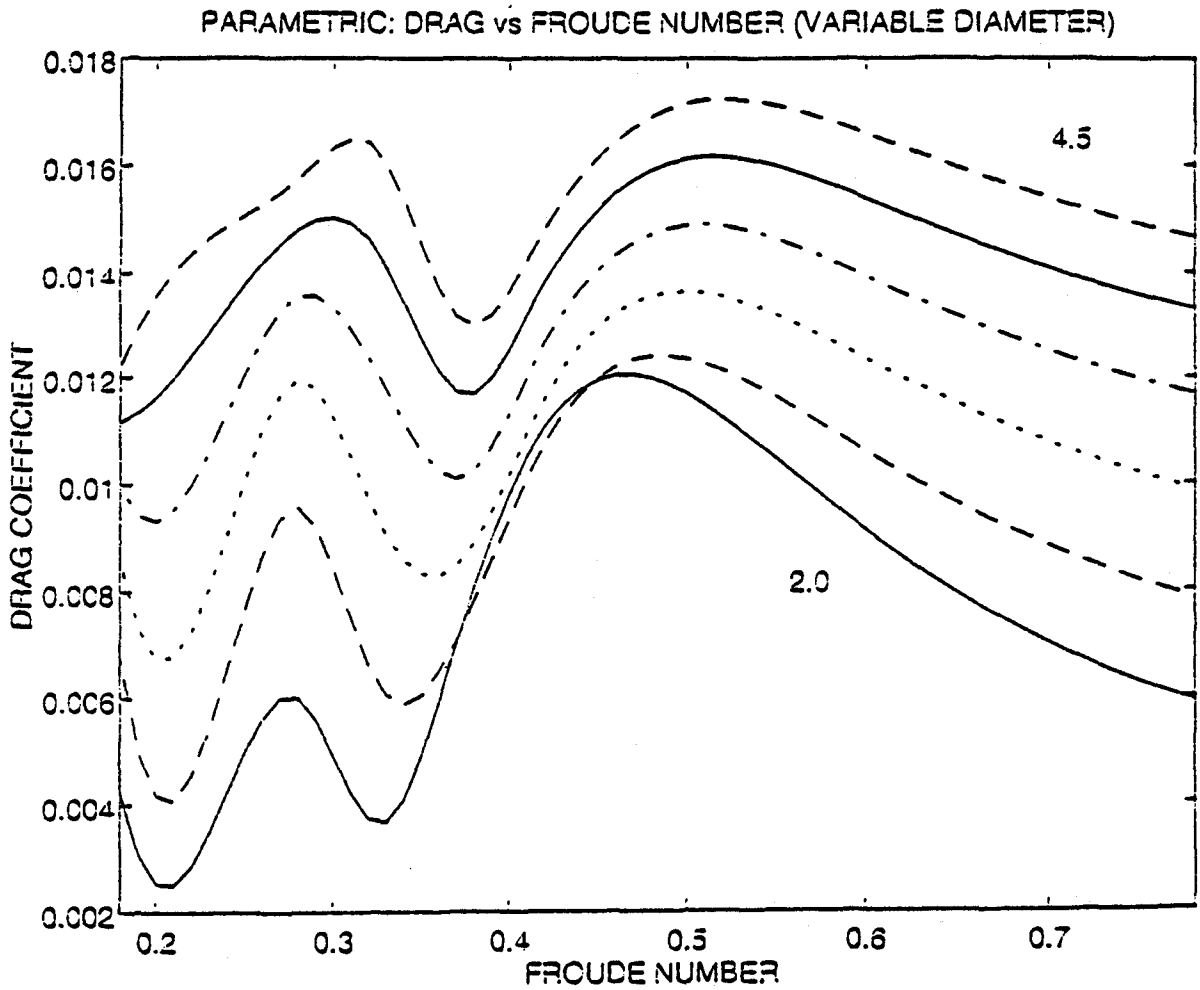

Figure 28: Parametric Study of Wave Making: Drag Coefficient versus Froude Number (Variable Diameter)

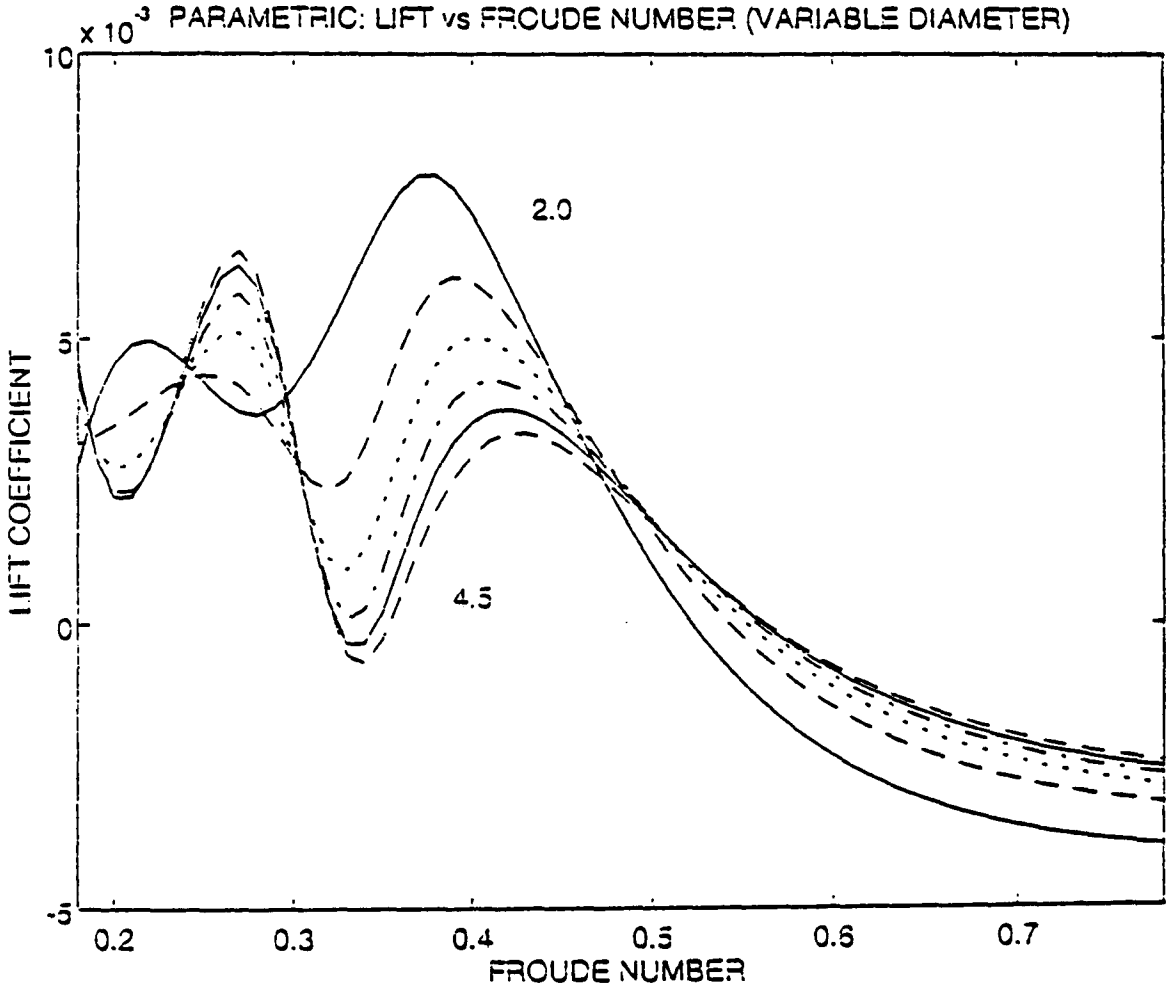

Figure 29: Parametric Study of Wave Making: Lift Coefficient versus Froude Number (Variable Diameter)

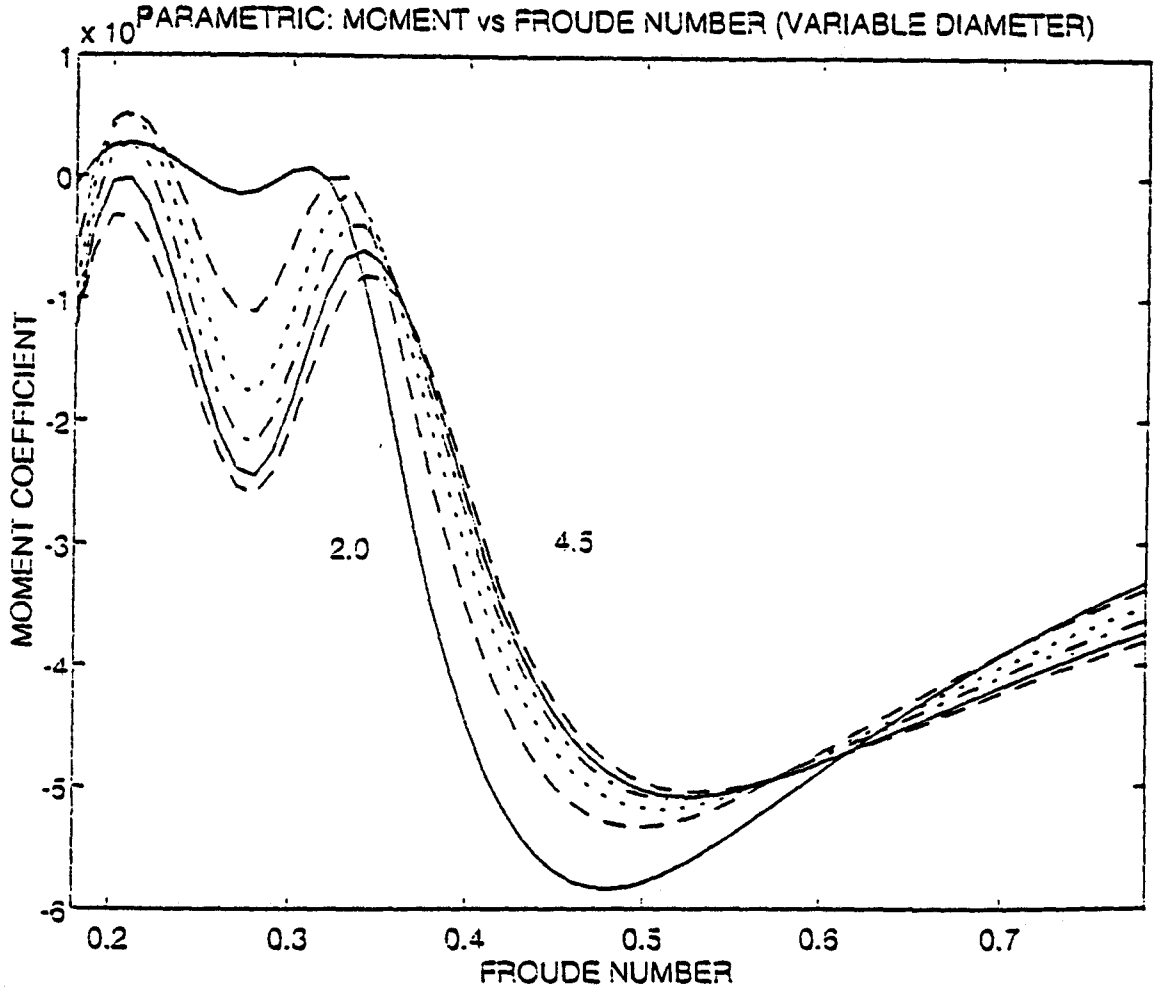

Figure 30: Parametric Study of Wave Making: Moment Coefficient versus Froude Number (Variable Diameter)

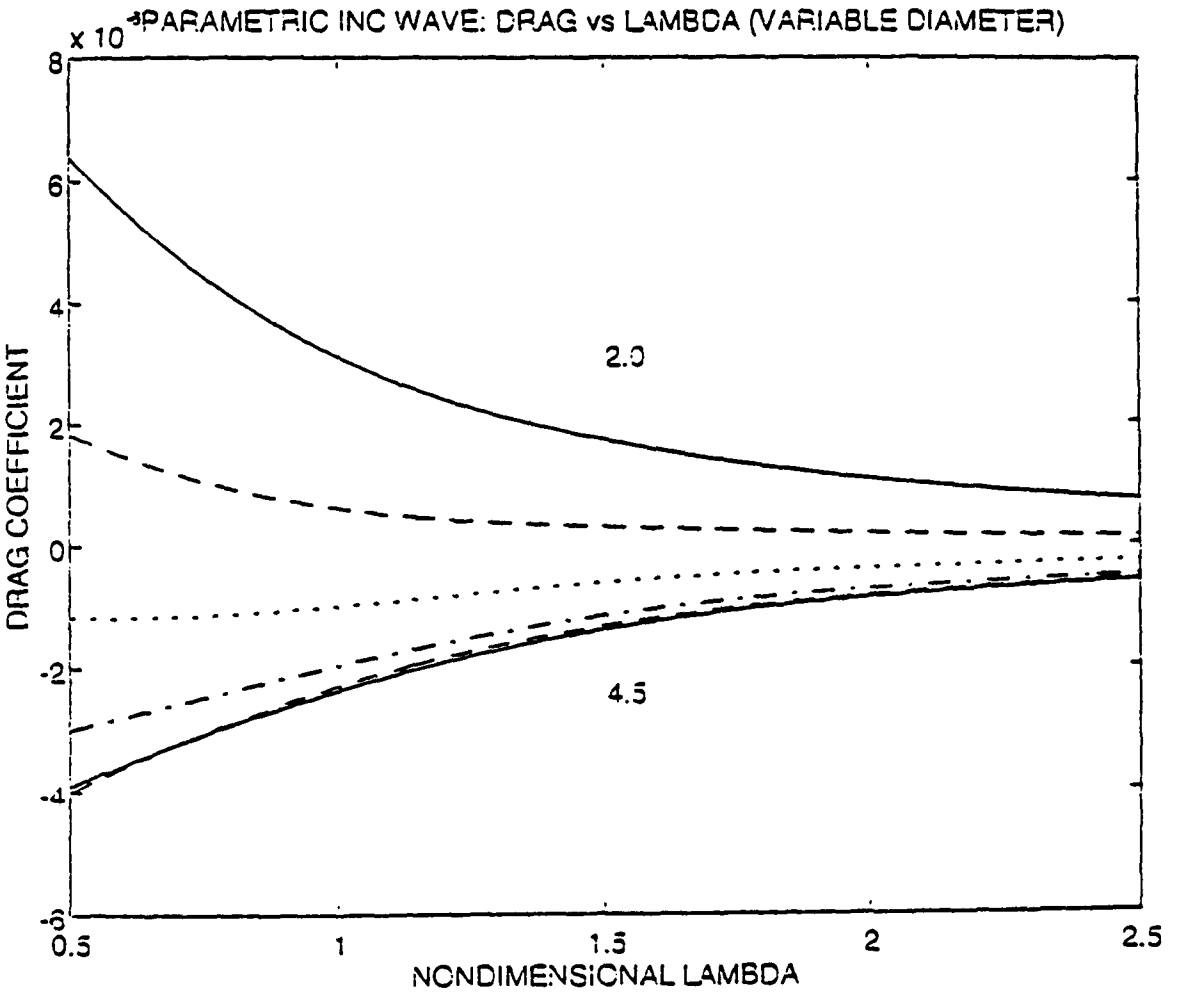

Figure 31: Parametric Study of Incident Waves: Drag Coefficient versus Nondimensional Wavelength (Variable Diameter)

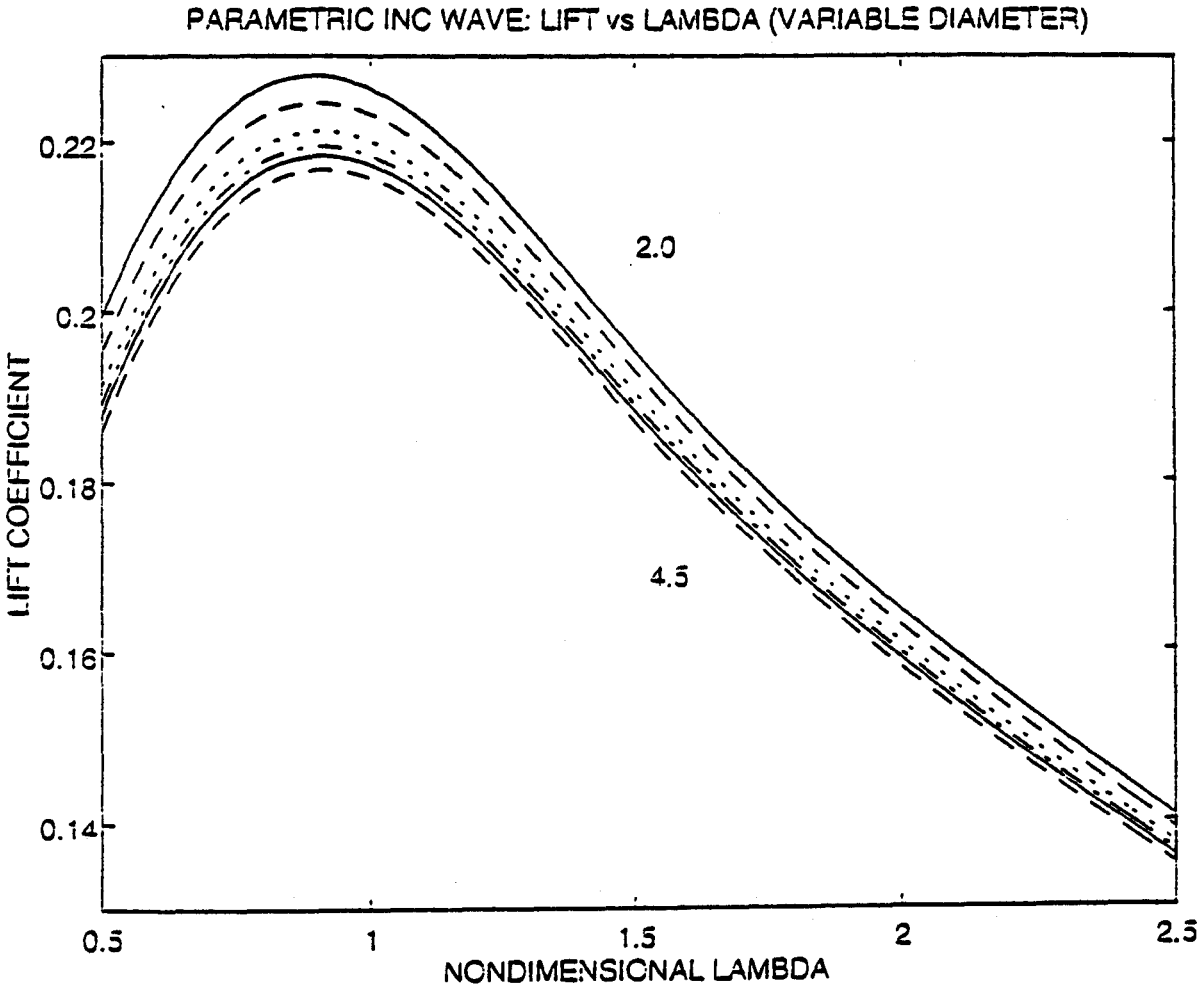

Figure 32: Parametric Study of Incident Waves: Lift Coefficient versus Nondimensional Wavelength (Variable Diameter)

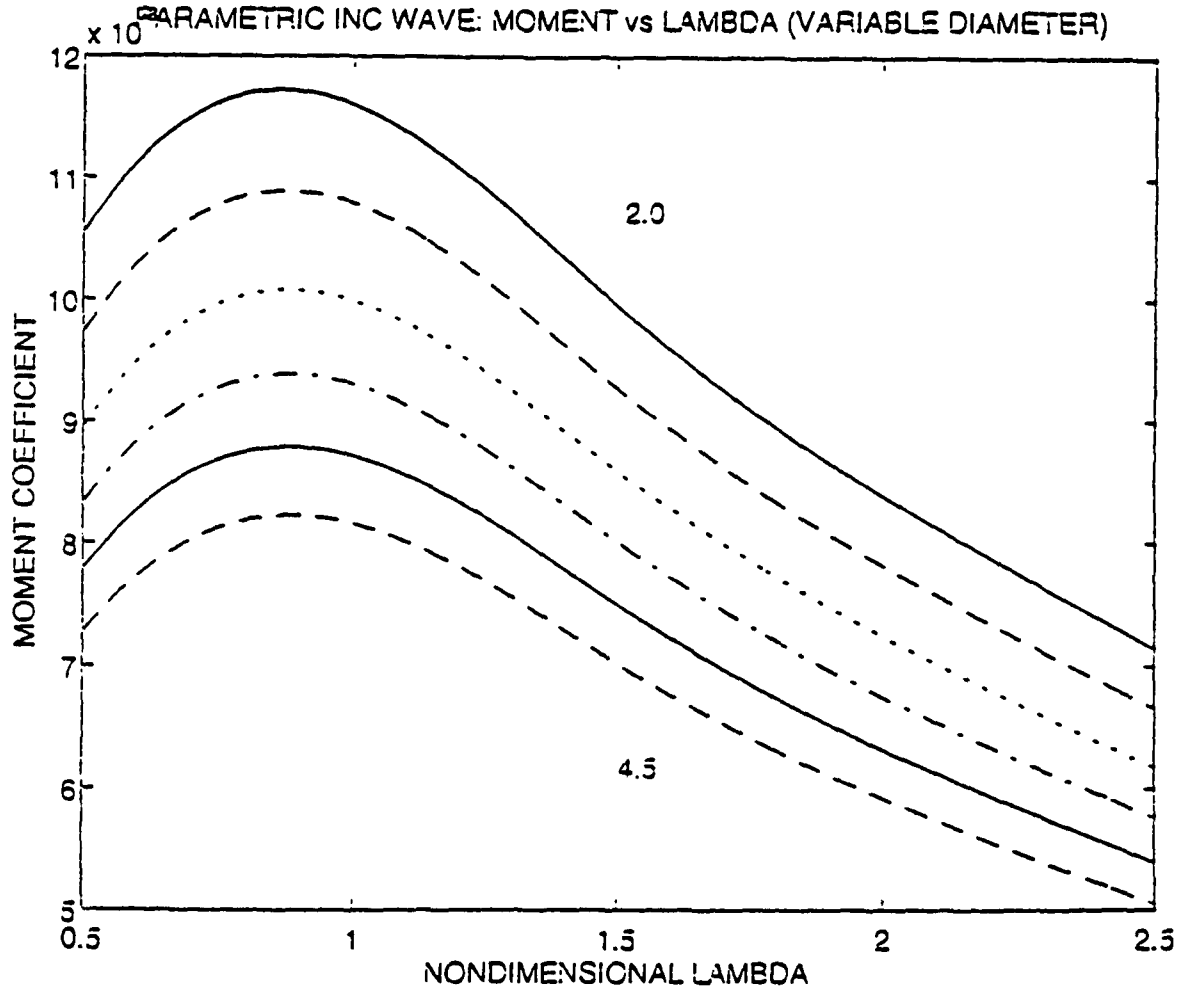

Figure 33: Parametric Study of Incident Waves: Moment Coefficient versus Nondimensional Wavelength (Variable Diameter)

V. CONCLUSIONS AND RECOMMENDATIONS

This work examined two significant free surface effects in a submerged body. The waves produced by the moving body interact with the free surface, and in turn, produce forces and a moment on the body. Secondly, the incident waves on the otherwise calm, free surface also produce its own forces and moment on the body. The combination of these two effects produce a total response on the body. The wave making effects were the major contributor to the body drag, causing a force which resisted the body's longitudinal motion. The incident waves produced the largest upwards lift force on the body, pulling the body to the free surface. A combination of the wave making and incident wave effects were responsible for the total bow-down moment on the body. Understanding these effects will aid the designer in optimizing future submarine designs and will assist submarine crews in effectively maintaining depth control at periscope depth. On the design side, the data from this work could be used directly in the simulation design based process or in design of an automatic depth control system. On the operational side, the data could be input into training simulators to better model the submarine operating at periscope depth. Additionally, the

results could be incorporated into the existing Ship's Fleet Mission Program Library (SFMPL) to aid the crew in trimming the submarine prior to proceeding to periscope depth.

To further improve the knowledge of free surface effects on submerged bodies, the following recommendations are proposed. First, the viscous effects in the body's boundary layer can be modelled to yield additional, significant forces and moments. These effects, especially flow separation from the body and its appendages would greatly add to the potential flow results discussed in this work. Secondly, the effects from the bottom or from other nearby sources (proximity effects) would likewise increase the accuracy of the resulting forces and moments. Finally, the effects of incident wave diffraction (which was neglected in this work) would produce additional forces and moments. Also, modelling the seaway as a random wave vice a sinusoidal wave would produce a more realistic seawave. These recommendations would serve to enhance the results presented in this work.

LIST OF REFERENCES

1. Bingham, B., F. Korsmeyer, J. Newman, "Prediction of the Seakeeping Characteristics of Ships", *Proceedings, 20th Symposium on Naval Hydrodynamics*, Santa Barbara, Ca., 1994.

2. Doctors, L., R. Beck, "Convergence Properties of the Neumann-Kelvin Problem for a Submerged Body", *Journal of Ship Research*, pp. 227-228, December 1987.

3. Hess, J., A. Smith, "Calculation of Nonlifting Potential Flow About Arbitrary Three-Dimensional Bodies", *Journal of Ship Research*, pp. 22-44, September 1964.

4. Jackson, H., "Fundamentals of Submarine Concepts Design", *SNAME paper*, pp. 15-4 - 15-5, October 1992.

5. Papoulias, F., "Dynamics of Marine Vehicles", *Informal Lecture Notes for ME 4823*, pp. 81-92, Naval Postgraduate School, Monterey, Ca., Summer 1993.

6. Papoulias, F., R. Beck, "WAVEAMP: A Program for Computation of Wave Elevations Created by a Ship Travelling at a Constant Speed", *Technical Report No. 88-03*, pp. 2-3, University of Michigan, Ann Arbor, Mi., July 1988.

7. Parsons, M., "NA420 Ship Resistance and Propulsion II", *Informal Notes*, pp.89-90, University of Michigan, Ann Arbor, Mi., Fall 1984.

8. Reed, A., R. Beck, O. Griffin, R. Peltzer, "Hydrodynamics of Remotely Sensed Surface Ship Wakes", *SNAME Transactions*, Vol 98, pp. 327,358-360, 1990.

9. Roddy, R., "Investigations of the Stability and Control Characteristics of Several Configurations of the DARPA SUBOFF Model (DTRC Model 5470) from Captive-model Experiments", *DTRC/SHD-1298-08*, pp.9-16, David Taylor Research Center, 1990.

INITIAL DISTRIBUTION LIST

		No. Copies
1.	Defense Technical Information Center Cameron Station Alexandria, VA 22304-6145	2
2.	Library, Code 52 Naval Postgraduate School Monterey, CA 93943-5002	2
3.	Chairman, Code ME Department of Mechanical Engineering Naval Postgraduate School Monterey, CA 93943-5000	1
4.	Professor F.A. Papoulias, Code ME/Pa Department of Mechanical Engineering Naval Postgraduate School Monterey, CA 93943-5000	5
5.	LCDR T.P. Crook, USN 11 Phythian Rd, Apt B Annapolis, MD 21402-1237	2
6.	Naval Engineering Curricular Office, Code 34 Naval Postgraduate School Monterey, CA 93943-5000	1
7.	H. Chatterton Director, Hull Form and Hydrodynamic Performance Division SEA 55W3 Naval Sea Systems Command Washington, DC 20360-5101	1